UNIVERSIDADE FEDERAL DE PERNAMBUCO
CENTRO DE CIÊNCIAS EXATAS E DA NATUREZA
PROGRAMA DE PÓS-GRADUAÇÃO EM FÍSICA

PAULO CÉSAR DO NASCIMENTO PEREIRA

FORCES ON DISLOCATIONS AND THE LIMITS OF CLASSICAL ELASTICITY IN 2D

Recife
2023

PAULO CÉSAR DO NASCIMENTO PEREIRA

FORCES ON DISLOCATIONS AND THE LIMITS OF CLASSICAL ELASTICITY IN 2D

Tese apresentada ao Programa de Pós-Graduação em Física da Universidade Federal de Pernambuco, como requisito parcial para obtenção do título de doutor em Física. Área de concentração: Física Teórica e Computacional.

Orientador: Sérgio Wlademir da Silva Apolinário

Recife

2023

Catalogação na fonte
Bibliotecária Nataly Soares Leite Moro, CRB4-1722

P436f Pereira, Paulo César do Nascimento
Forces on dislocations and the limits of classical elasticity in 2D / Paulo César do Nascimento Pereira. – 2023.
77 f.: il., fig., tab.

Orientador: Sérgio Wlademir da Silva Apolinário.
Tese (Doutorado) – Universidade Federal de Pernambuco. CCEN, Física, Recife, 2023.
Inclui referências.

1. Física teórica e computacional. 2. Física do estado sólido. 3. Cristais bidimensionais. 4. Teoria da elasticidade. 5. Plasticidade. 6. Dislocations I. Apolinário, Sérgio Wlademir da Silva (orientador). II. Título.

530.1 CDD (23. ed.) UFPE- CCEN 2023 - 190

PAULO CÉSAR DO NASCIMENTO PEREIRA

FORCES ON DISLOCATIONS AND THE LIMITS OF CLASSICAL ELASTICITY IN 2D

Tese apresentada ao Programa de Pós-Graduação em Física da Universidade Federal de Pernambuco, como requisito parcial para a obtenção do título de Doutor em Física.

Aprovada em: 21/03/2023.

BANCA EXAMINADORA

_____
Prof. Sérgio Wlademir da Silva Apolinário
Orientador
Universidade Federal de Pernambuco

_____
Prof. Antônio Murilo Santos Macêdo
Examinador Interno
Universidade Federal de Pernambuco

_____
Prof. José Albino Oliveira de Aguiar
Examinador Interno
Universidade Federal de Pernambuco

_____
Prof. Hartmut Löwen
Examinador Externo
Heinrich Heine University Düsseldorf

_____
Prof. Milorad Milošević
Examinador Externo
University of Antwerp

AGRADECIMENTOS

Aos meus pais Fábio e Telma, à minha avó Terezinha, à minha irmã Débora e ao meu sobrinho Arthur Marx por todo o apoio sempre presente durante a jornada de doutorado. Ao meu orientador Dr. Sérgio Apolinário pela orientação, apoio e paciência. Ao meu colega de laboratório Everton Lima e a outros amigos da UFPE pelas proveitosas conversas. Aos Drs. Antônio Murilo Macêdo, José Albino Aguiar, Hartmut Löwen e Milorad Milošević pelos comentários e sugestões na finalização desta tese. Agradeço também aos secretários da pós-graduação Alexsandra Melo e Ailton Silva por todo suporte fornecido durante o doutorado. Aos familiares e amigos que me davam apoio mesmo sem entender muito bem este meu trabalho. Por fim, à FACEPE, à CAPES e ao CNPq pelo apoio financeiro que deram ao longo da minha formação.

ABSTRACT

This thesis investigates some limits of the classical theory of elasticity in 2D, especially concerning forces on topological defects called dislocations. Initially, the thesis comments each approximating step used in deriving Classical Elasticity. Novel discussions are made about the continuum assumption and the limits of the sum-to-integral approximation. Moreover, an alternative mathematical formalism to deformations in 2D is introduced in order to obtain simpler equations and physical inferences. Thereafter, the notion of the core force is studied. This is a correction to the classical force on dislocation, called Peach-Koehler force, and which appears when in the presence of strain gradients. It has been predicted by different approaches but never observed, until a work which is presented in this thesis. A simulation model to investigate such force and its results are shown. By comparing with the previous theoretical approaches, it is verified that none of them is capable of providing a way to quantitatively predict the core force. Furthermore, it is shown that, for some systems, results from the core force can be used to predict a definite value for the core energy of the dislocation.

Keywords: solid state physics; two-dimensional crystals; elasticity theory; plasticity; dislocations.

RESUMO

Esta tese investiga alguns limites da teoria clássica da eslasticidade em 2D, especialmente no que concerne a forças em defeitos topológicos chamados dislocations. Inicialmente, a tese comenta cada passo de aproximação usado ao se derivar a Elasticidade Clássica. Novas discussões são feitas sobre a suposição do contínuo e sobre os limites de sua aproximação soma-para-integral. Adicionalmente, um formalismo matemático alternativo para deformações em 2D é introduzido a fim de obter equações e inferências física mais simples. Após isso, a noção de força do “core” é estudada. Esta é uma correção à força clássica cobre um dislocation, chamada força de Peach-Koehler, e que apareça quando na presença de gradientes de deformação. Ela tinha sido prevista por diferentes abordagens, mas nunca observada, até um trabalho que é apresentado nesta tese. Um modelo de simulação para investigar esta força e seus resultados são mostrados. Ao comparar com as abordagens teóricas anteriores, verifica-se que nenhuma delas é capaz de fornecer uma forma de prever quantitativamente a força do “core”. Além disso, é mostrado que, para alguns sistemas, resultados desta força podem ser usados para prever um valor definido para a chamada energia do “core” de um dislocation.

Palavras-chave: física do estado sólido; cristais bidimensionais; teoria da elasticidade; plasticidade; dislocations.

CONTENTS

1 INTRODUCTION

This thesis explores elastic and plastic deformations in two-dimensional (2D) crystals. The examination of dislocations and their dynamics emerged as a compelling avenue to probe the boundaries of Classical Elasticity Theory and other potential continuum theories. Several chapters in this work draw heavily from the article “Forces on dislocations due to strain gradients: theories and 2D simulations” (PEREIRA, 2022), while others introduce noteworthy discussions that remain unpublished.

1.1 STRUCTURE OF THE THESIS

This section serves as a roadmap, offering a comprehensive overview of each segment within the thesis. For a detailed exploration of novel findings and their prospects, please refer to the conclusions provided in section 8.2.

Section 1.2 introduces the concept of dislocations and their dynamics, drawing heavily from the introductory material presented in (PEREIRA, 2022). Prior to delving into the examination of forces acting on dislocations, the subsequent chapters establish the foundational equations of Classical Elasticity. To ensure precision in the theoretical framework, we commence with first principles, meticulously detailing each approximation made.

In chapter 2, we present the mathematical portrayal of deformations, initially in 1D and subsequently in 2D. Section 2.1.1 covers fundamental concepts related to deformation, displacement, and strain. Section 2.1.2 incorporates a continuum assumption and defines both Lagrangian and Eulerian descriptions. Section 2.1.3 delves into key aspects of the strain field, while section 2.1.4 addresses the significance of regularizing continuum fields. Section 2.1.5 introduces a regularization procedure that establishes valuable sum-to-integral equivalences.

In section 2.2.1, we extend the definitions of displacements and strains to 2D crystals and introduce the concept of dislocation. Section 2.2.2 elucidates the meaning of each strain component. Section 2.2.3 puts forth an alternative mathematical formalism that offers advantages in addressing dislocations. Section 2.3 defines and explores the topological charge associated with a dislocation.

Chapter 3 delves into the physics of elasticity within specific approximations, commencing with discussions on energy and culminating in exact results regarding dislocations. Section 3.1.1 defines the type of particles' interaction potential considered throughout this thesis. Section 3.1.2 explores deformations within the crystal, incorporating relevant approximations. Section 3.1.3 evaluates the interaction energy resulting from deformation, assumes continuity, and employs regularization to establish sum-to-integral equivalences. Section 3.1.4 extends this analysis to external potentials. Section 3.1.5 sums up these results, presenting the equations of Classical Elasticity.

In section 3.2.1, we derive the classical formula for the force acting on a dislocation due to background deformations. Section 3.2.2 defines dislocation glide, demonstrating it as the sole dislocation motion preserving the total particle number. Section 3.2.3 utilizes the formalism introduced in section 2.2.3 to derive simplified equations of Classical Elasticity for triangular crystals. We discuss how the dynamics of dislocations can lead to the formation of conformal crystals. Section 3.2.4 extends this exploration by deriving classical Volterra solutions for the deformation of a dislocation.

The text from section 3.2.5 to 8.1 is strongly based on the article (PEREIRA, 2022) published by the present author. Section 3.2.5 obtains some results for a dipole of dislocations in a box with PBC, which will be usefull for the simulations. Chapter 4 establishes fundamental assumptions about the core force, enumerates its properties, and deliberates on simulation methodologies. Section 4.1.1 underscores the non-obvious nature of the core force's effective existence. Section 4.1.2 defines the driving force on a dislocation as the sum of the Peach-Koehler (PK) force and the core force, serving as a correction beyond Classical Elasticity. Sections 4.1.3 and 4.1.4 catalog and discuss various properties of the core force to be explored through simulations. Section 4.1.5 introduces new discussions on how the core force's interactions between dislocations can induce size effects and nonreciprocity. Section 4.2.1 examines precautions essential for achieving precision in simulations, covering aspects such as dislocation position, background strains, and core force magnitude.

Chapter 5 meticulously outlines our simulation setup and presents its outcomes. The discussion highlights how choices related to interparticle interactions (section 5.1.1), boundary conditions (section 5.1.2), dislocation configuration (section 5.1.3), and external force (section 5.1.4) serve to validate key properties of the core

force while ensuring precision in measuring its magnitude. Section 5.2 unveils the results, demonstrating that an expression for the core force, comprised of terms involving first and third derivatives of background strains, aligns well with the simulation data.

After obtaining results from simulations, chapters 6 and 7 undertake a comparative analysis with various theoretical approaches. Section 6.1 elucidates how a core force can be derived from a core energy dependence on background strains. The core energy is defined in section 6.1.1 for general cases, independent of the chosen continuum theory. Section 6.1.2 utilizes Classical Elasticity to derive the standard core energy, revealing inherent ambiguities. In section 6.1.3, the core energy of systems with power-law interactions is explored, establishing a direct relation between this energy and the coefficients of the core force based on the scaling law of these systems. Alternatively, section 6.2 examines modifications to the classical energy functional, including nonlinear and higher gradient terms, and analyzes their implications for corrections to the PK force. However, none of these modifications satisfy the properties observed in the simulations.

Chapter 7 delves into the core field approach, a modification in the description of dislocations within continuum theory. Section 7.1 defines the core field, providing a formula for the core force derived from it, satisfying all observed properties in the simulations. Subsequently, in section 7.2, we present a method to measure the core field through simulations. However, the results indicate that this approach cannot be used to predict the coefficients of the core force measured in chapter 5.

Finally, the comparisons between theories and simulations of the core force are summarized in section 8.1. Section 8.2 offers an overview of our key novel results and presents some perspectives for future exploration.

1.2 INTRODUCTION TO THE CORE FORCE IDEA

The idea of dislocation defects was first conceived mathematically (VOLTERRA, 1907) and later applied in the context of plasticity (TAYLOR, 1934), by considering the movement of defects in a periodic lattice. It soon became a vital feature of investigation in real three-dimensional (3D) crystals (FRANK, 1952; HIRTH; LOTHE, 1982; KUBIN, 2013). Since the bubble-raft model (BRAGG; NYE, 1947), 2D crystals have also been used as simple models to study dislocation

dynamics (e.g., using colloids (VAN DER MEER et al., 2014), complex plasmas (NOSENKO; MORFILL; ROSAKIS, 2011) and vortices in superconductors (MIGUEL; ZAPPERI, 2013)). Figure 1 shows an experimental example of a 2D crystal after a plastic deformation during which the dislocations moved in order to minimize the energy.

Figure 1 – Configuration of magnetized steel balls in a thin and tilted box. These balls have dipole-dipole repulsion and forms a crystal when confined. The gravity induces deformation in the crystal while tilting the box. During such deformation, dislocations can move, nucleate and annihilate. The final “gravity rainbow” pattern (PIERAŃSKI, 1989) has few remaining dislocations, which are highlighted in this image by the blue circles.

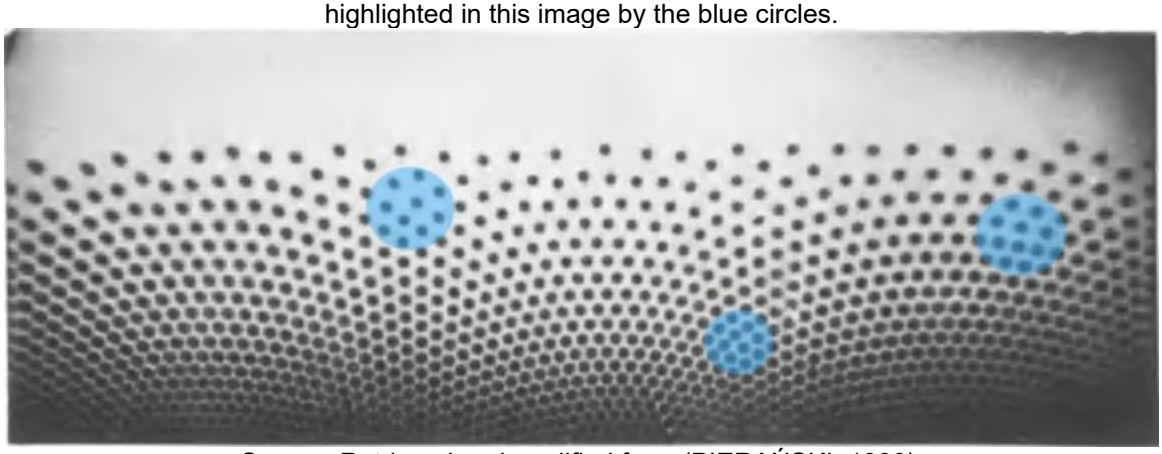

Source: Retrieved and modified from (PIERAŃSKI, 1989).

The individual dislocation movement is generally assumed to be governed by some well-known mechanisms: the **Peach-Koehler (PK) driving force** (PEACH; KOEHLER, 1950) and the **Peierls-Nabarro barrier** (PEIERLS, 1940; NABARRO, 1947) besides other possible motion's resistance, climb and diffusion mechanisms (HIRTH; LOTHE, 1982; PHILLIPS, 2001; BULATOV, 2006; KUBIN, 2013). These forces have been widely used to model plastic deformations in Discrete Dislocation Dynamics (DDD) simulations (BULATOV, 2006, KUBIN, 2013), where the exact locations of all atoms can be ignored and one only needs to consider the dynamics of dislocation lines, in 3D, or points, in 2D. The validity of such mesoscale approach relies on the forces and mobility law that it considers.

The mechanisms cited above cannot fully explain the full range of new plastic phenomena with technological impact observed, e.g., in micron and sub-micron scales (GREER, 2011; KRAFT et al., 2010; GAO; BEI, 2016; VOYIADJIS; YAGHOOBI, 2017; VOYIADJIS; YAGHOOBI, 2019) (with a “smaller is stronger” trend) and during shock loadings (MEYERS et al., 2009; REMINGTON; RUDD; WARK, 2015; ZEPEDA-RUIZ et al., 2017; WEHRENBERG, 2017; SLIWA et al.,

2018; MISHRA et al., 2021). These are situations where high strain gradients and strain rates appear. As a consequence, several phenomenological and mechanism-based models have been developed, including corrections to the mobility law (GURRUTXAGA-LERMA, 2016), nonlocal Elasticity (ERINGEN, 2002; LAZAR, 2005) and strain gradient plasticity (AIFANTIS, 1992; HUTCHINSON; FLECK, 1997; HUANG et al., 2004; FLECK; HUTCHINSON; WILLIS, 2015; VOYIADJIS; SONG, 2019).

E. Clouet (CLOUET, 2011) observed that the usual mathematical representation for the origin of the so-called **core field** leads to a fundamentally different type of driving force on a dislocation. It is a force proportional to the derivatives of the **background strains**, which are the ones generated by all sources of strain but the dislocation itself. Such type of force has been called the **core force** and can contribute, in a fundamental manner, for the emergence of strange phenomena when high strain gradients are present. Clouet's theoretical framework predicted a relation between the coefficients of the core force and the ones of the core field.

Another approach for the core force was made by M. Iyer et al. (IYER; RADHAKRISHNAN; GAVINI, 2015), considering that the core force can be viewed as originated from the interaction of the core with the background strains. They developed an Electronic-structure evaluation of the core energy, in its standard definition, for different background strains. They used this to predict the coefficients of the core force that can act on the dislocation. But they do not discuss about the ambiguity due to the arbitrariness of the core radius present in the standard core energy definition.

The aim of our work is to broaden current knowledge about the core force. In spite of the previous theoretical works, such type of force has not been directly observed and identified, neither through simulations nor through experiments. It is usually very smaller than PK and to identify it one needs the precise knowledge of both the strains and the resulting force on a dislocation. To meet this requirement, we design, in the present work, a 2D system where these variables are completely known. We simulate it, demonstrating the existence, probing the properties and measuring the coefficients of the core force on edge dislocations.

By analyzing simulations and theories, we found that the current theoretical proposals for the core force are insufficient to explain or predict the results of our 2D

simulations. This is summarized in section 8.1 and shown in a table. We observed that, e.g., Clouet's approach has quantitative problems and the one used by Iyer et al. is ill-defined.

As another discovery, we observe that, in systems with scale invariance such as the one in our simulations, the core energy can be obtained directly from the core force coefficients. A definite value for this quantity is obtained although the core energy is usually defined in an ambiguous manner. This unambiguous evaluation can be compared with other studies which need or predict the existence of a specific core energy with physical meaning, such as the KTHNY-theory for 2D melting (STRANDBURG, 1988) and the Kanzaki force approach to represent crystalline defects (GURRUTXAGA-LERMA; VERSCHUEREN, 2019).

2 MATHEMATICAL DESCRIPTION OF DEFORMATIONS

This chapter discusses some notions about deformations in one-dimensional (1D) crystals, where some definitions can be easily introduced, and in 2D ones, where topological defects can appear. Here we propose a deeper analysis of discrete-to-continuum transitions and a new mathematical formalism for 2D deformations.

2.1 1D CHAIN

Lets start considering a system with N particles placed in a **perfect 1D chain** which are **spaced by a_0 from their neighbors**.

2.1.1 Deformation of a 1D perfect chain and displacement of its constituents

The **particles are then displaced** from their positions $\{X^{(\alpha)}\}$ in the undeformed chain **to new positions** $\{x^{(\alpha)}\}$, where superscript indexes with greek letters in parentheses are used as particle labels. Here, neither a particle was inserted or removed in the system nor there happened a superposition of particles. Therefore, the **deformation** $X^{(\alpha)} \mapsto x^{(\alpha)}$ is a **bijective (one-to-one) mapping**, where $\alpha \in \{1, 2, ..., N\}$. From this map, we define the **displacement** $u^{(\alpha)}$ of particle α as

$$u^{(\alpha)} = x^{(\alpha)} - X^{(\alpha)}. \tag{2.1}$$

Note that, if all displacements are equal, the deformation is simply a rigid body translation. We are not interested in such trivial case as well as in cases of simply interchanges of particles' positions (for instance, $x^{(\alpha)} = X^{(\beta)}$ and $x^{(\beta)} = X^{(\alpha)}$ for some $\alpha \neq \beta$). **The physically relevant deformations are the ones that strains the system**, that is, when there are regions where the interparticles' distances were compressed or stretched. The physical relevance here comes from the fact that the energy depends on these interparticles' distances, as we will consider in the next chapter. In strained systems, particles α and β whose distance changed have different displacements since, from equation (2.1),

$$x^{(\alpha)} - x^{(\beta)} \neq X^{(\alpha)} - X^{(\beta)} \quad \Longleftrightarrow \quad u^{(\alpha)} - u^{(\beta)} \neq 0. \tag{2.2}$$

2.1.2 Continuum assumption and the Lagrangian and Eulerian descriptions

For the bijective map $X^{(\alpha)} \mapsto x^{(\alpha)}$, defined in a finite discrete set of points, **there exist a continuous and bijective function** $x(X)$ **satisfying**

$$x(X^{(\alpha)}) = x^{(\alpha)} \quad \forall \alpha \in \{1, 2, ..., N\}. \tag{2.3}$$

This is equivalent to **considering the undeformed and deformed chains as continuum systems** and the deformation as a continuous and invertible map $x(X)$. This is the **continuum assumption**, which usually considers that the function $x(X)$ is also smooth, that is, infinitely differentiable.

Note that, within the continuum assumption, the deformation is equivalent to a change of variables or a coordinate transformation between the undeformed coordinates X and the deformed coordinates x. We define the **Lagrangian displacement field** by taking the displacement as a function of the undeformed positions, that is,

$$u^{\mathrm{L}}(X) = x(X) - X \quad \text{satisfying} \quad u^{\mathrm{L}}(X^{(\alpha)}) = u^{(\alpha)} \quad \forall \alpha, \tag{2.4}$$

and the **Eulerian displacement field** as a function of the deformed positions, that is,

$$u^{\mathrm{E}}(x) = x - X(x) \quad \text{satisfying} \quad u^{\mathrm{E}}(x^{(\alpha)}) = u^{(\alpha)} \quad \forall \alpha, \tag{2.5}$$

where $X(x)$ is the inverse of the bijection $x(X)$.

In Elasticity Theory, we make use of the continuum assumption in order obtain simpler equations for the physics of deformation, which can be in the Lagrangian description (i.e., using the undeformed positions X as variables) or in the Eulerian one (i.e., using the undeformed positions x as variables).

2.1.3 Strain field

In practice, the continuum assumption in the equations of Elasticity Theory is convenient to make some approximations. For example, for nearby particles α and β, we can approximate

$$u^{(\beta)} - u^{(\alpha)} \approx \left[X^{(\beta)} - X^{(\alpha)}\right] \frac{\mathrm{d}u^{\mathrm{L}}}{\mathrm{d}X}(X^{(\alpha)}) \approx \left[x^{(\beta)} - x^{(\alpha)}\right] \frac{\mathrm{d}u^{\mathrm{E}}}{\mathrm{d}x}(x^{(\alpha)}). \tag{2.6}$$

From this equation and from the discussion in the end of section 2.1.1, we can see that a nonzero derivative of the displacement field is associated with a straining of the system. Thus, we define the **Lagrangian and Eulerian strain fields** as, respectively,

$$\varepsilon^{\mathrm{L}}(X) = \frac{\mathrm{d}u^{\mathrm{L}}}{\mathrm{d}X}(X) \quad \text{and} \quad \varepsilon^{\mathrm{E}}(x) = \frac{\mathrm{d}u^{\mathrm{E}}}{\mathrm{d}x}(x). \tag{2.7}$$

Note that the Lagrangian and Eulerian displacement fields evaluated for the same particle are equal, i.e., $u^{\mathrm{L}}(X^{(\alpha)}) = u^{\mathrm{E}}(x^{(\alpha)}) \ \forall\alpha$, but the respective strain fields are not equal. In fact, from equations (2.4) and (2.5),

$$\varepsilon^{\mathrm{L}}(X^{(\alpha)}) = \frac{\mathrm{d}x}{\mathrm{d}X}(X^{(\alpha)}) - 1 \tag{2.8}$$

and

$$\varepsilon^{\mathrm{E}}(x^{(\alpha)}) = 1 - \frac{\mathrm{d}X}{\mathrm{d}x}(x^{(\alpha)}) = 1 - \left[\frac{\mathrm{d}x}{\mathrm{d}X}(X^{(\alpha)})\right]^{-1} = \varepsilon^{\mathrm{L}}(X^{(\alpha)}) \left[1 + \varepsilon^{\mathrm{L}}(X^{(\alpha)})\right]^{-1} \neq \varepsilon^{\mathrm{L}}(X^{(\alpha)}). \tag{2.9}$$

In the limit of small strains, which is considered in Linear Elasticity Theory, terms of second order or higher in strains are neglected and we have $\varepsilon^{\mathrm{L}}(X^{(\alpha)}) = \varepsilon^{\mathrm{E}}(x^{(\alpha)})$. Thus, we can **simplify the notation in the limit of Linear Elasticity**, omitting the superscript and considering the type of position variables as indicator of the description, that is,

$$u(X) \equiv u^{\mathrm{L}}(X), \quad \varepsilon(X) \equiv \varepsilon^{\mathrm{L}}(X), \quad u(x) \equiv u^{\mathrm{E}}(x) \quad \text{and} \quad \varepsilon(x) \equiv \varepsilon^{\mathrm{E}}(x). \tag{2.10}$$

From now on, we will use this notation unless there is a need to be explicit.

Finally, in spite of defining the strain field through the displacement field, we can start by using some way to define **discrete strains**, such as

$$\varepsilon^{(\alpha)} = \frac{u^{(\alpha+1)} - u^{(\alpha)}}{a_0} \quad \text{or} \quad \varepsilon^{(\alpha)} = \frac{u^{(\alpha+1)} - u^{(\alpha-1)}}{2a_0}, \tag{2.11}$$

and thereafter make a continuum assumption to define a continuum field $\varepsilon(X)$ which satisfies $\varepsilon(X^{(\alpha)}) = \varepsilon^{(\alpha)}$. The displacement field can then be obtained by integrating this strain field and using boundary conditions. In this case, the obtained $u(X)$ does not necessarily obeys the constraints $u(X^{(\alpha)}) = u^{(\alpha)}$. On the other side, we can start defining $u(X)$ from $u^{(\alpha)}$ then obtain $\varepsilon(X)$ by differentiation, arriving at a strain field which does not necessarily obey the constraints $\varepsilon(X^{(\alpha)}) = \varepsilon^{(\alpha)}$. In general, we choose to start defining $\varepsilon(X)$ from its discrete values, since the elasticity theory depends more on strains than it depends on displacements.

2.1.4 Regularization and the sum-to-integral approximation

It is important to note that there are infinite possibilities to define a continuum field from discrete points. Figure 2 shows examples of different continuum functions that matches discrete points. We can use the physical constraint that **particles**

cannot be on the same place or pass through each other during deformation, that implies in $\mathrm{d}x/\mathrm{d}X > 0$ and thus

$$\varepsilon(X) > -1. \tag{2.12}$$

almost everywhere. Moreover, in a crystal with N particles under **periodic boundary conditions (PBC)**, which represents an infinite crystal with

$$X^{(\alpha)} = \alpha a_0,\ \alpha \in \mathbb{Z}, \qquad u^{(\alpha+N)} = u^{(\alpha)} \quad \text{and} \quad \varepsilon^{(\alpha+N)} = \varepsilon^{(\alpha)}, \tag{2.13}$$

we have the following **constraints due to periodicity**

$$u(X+L) = u(X),\ \ \varepsilon(X+L) = \varepsilon(X) \ \text{ and } \int_0^L \varepsilon(X)\mathrm{d}X = 0, \tag{2.14}$$

where $L = Na_0$ is the crystal's size. Nevertheless, there are sill room for infinite possibilities of continuum functions. Additional conditions can be considered in order to define how to obtain a more appropriate continuum function which interpolates the points associated with the deformed crystal. In Mathematics and Data Science, this process is called **regularization**.

Figure 2 – Many different continuum functions can match at a discrete set of points.

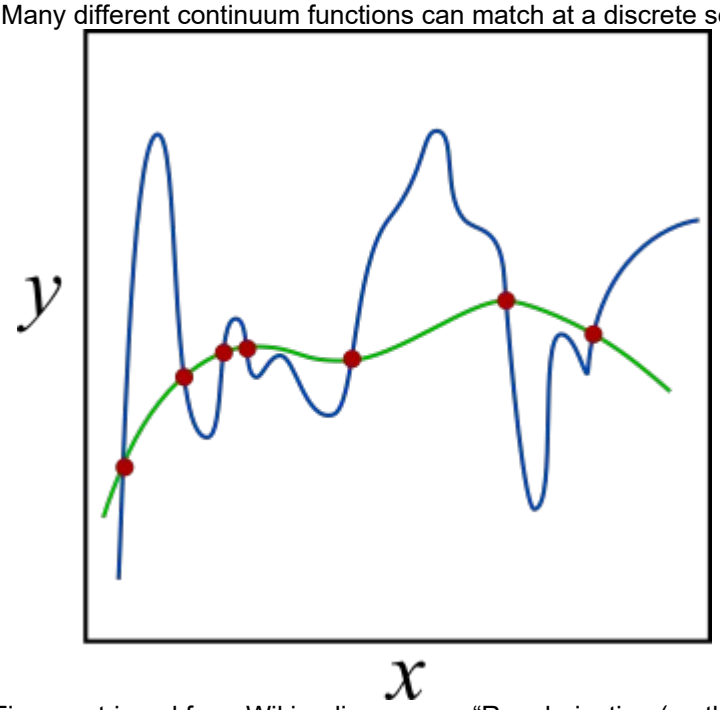

Source: Figure retrieved from Wikipedia page on “Regularization (mathematics)” (<https://en.wikipedia.org/wiki/Regularization_(mathematics)>, 2023).

Lets consider the strain field. First we need it to be **smooth in the mathematical sense**, that is, infinitely differentiable. This allows us to make the expansion

$$u^{(\beta)} - u^{(\alpha)} = u(X^{(\beta)}) - u(X^{(\alpha)}) = \sum_{n=0}^{\infty} \frac{\left[X^{(\beta)} - X^{(\alpha)}\right]^{n+1}}{n!} \frac{\mathrm{d}^n \varepsilon}{\mathrm{d}X^n}(X^{(\alpha)}). \tag{2.15}$$

We will use only the first term of the expansion to derive the Classical Elasticity in chapter 3 and add the second term to derive a Strain Gradient Theory in chapter 6. Therefore, we also need the strain field to be **smooth in the common sense**, that is, with less "roughness" that are associated with fluctuations within small wavelengths. For instance, the green function in figure 2 is smoother than the blue one. This type of smoothness makes the terms with higher derivatives in equation (2.15) to decay rapidly to zero, providing us good perturbative approximations.

Another condition for the continuum strain field to be appropriate for our purposes is to provide good **sum-to-integral approximations**, that is,

$$\sum_{\alpha=1}^{N} f\big(\varepsilon^{(\alpha)}\big) = \sum_{\alpha=1}^{N} f\big(\varepsilon(X^{(\alpha)})\big) \approx \int_0^L f\big(\varepsilon(X)\big)\rho_0 \mathrm{d}X, \tag{2.16}$$

where f is some smooth function and $\rho_0 = 1/a_0$ is the 1D particle density and we used $X^{(\alpha)} = \alpha a_0$. For small strains, we can perturbatively expand f and consider only sums of the small powers of ε.

2.1.5 A proposal for regularization

We propose a way to obtain a strain field which is smooth (in the common sense) and provides some sum-to-integral equivalences. This regularization is possible in a crystal under PBC, for which we can write the strain field as a Fourier series in such a way that it avoids terms with large wavelengths, thus avoiding unnecessary roughness. For it, we first use the **discrete Fourier transform**

$$\hat{\varepsilon}^{(n)} = \frac{1}{N} \sum_{\alpha=1}^{N} \varepsilon^{(\alpha)} e^{-i\frac{2\pi n \alpha}{N}} \tag{2.17}$$

to obtain the coefficients of the following **Fourier series**

$$\varepsilon^{\mathrm{F}}(X) = \sum_{n=1-N/2}^{N/2} \mathrm{Re}\left[\hat{\varepsilon}^{(n)} e^{i\frac{2\pi n X}{L}}\right] \tag{2.18}$$

$$= \hat{\varepsilon}^{(0)} + \sum_{n=1}^{N/2-1} 2\left[\mathrm{Re}\big[\hat{\varepsilon}^{(n)}\big]\cos\left(\frac{2\pi n X}{L}\right) - \mathrm{Im}\big[\hat{\varepsilon}^{(n)}\big]\sin\left(\frac{2\pi n X}{L}\right)\right] + \hat{\varepsilon}^{(N/2)}\cos\left(\frac{\pi X}{a_0}\right), \tag{2.19}$$

where $\mathrm{Re}[z]$ and $\mathrm{Im}[z]$ are the real and imaginary parts of z. One can see that $\varepsilon^{\mathrm{F}}(X^{(\alpha)}) = \varepsilon^{(\alpha)}$ by using equations (2.17) and (2.18) and $\sum_{n=1-N/2}^{N/2} e^{i\frac{2\pi n \alpha}{N}} = N\delta_{\alpha 0}$,

where δ_{ij} is the **Kroenecker delta** (equals to 1 if $i=j$ and 0 if $i\neq j$). Note that, due to the PBC, $\hat{\varepsilon}^{(0)}=0$ for both definitions of $\{\hat{\varepsilon}^{(\alpha)}\}$ in equation (2.11), while $\hat{\varepsilon}^{(N/2)}=0$ for the second one. We consider the general case since these identities may not hold for other definitions, especially when we generalize to 2D crystals.

The function in equation (2.18) is a Fourier series representation which optimizes the avoiding of unnecessary roughness. However, if $\hat{\varepsilon}^{(0)}\neq 0$ or $\hat{\varepsilon}^{(N/2)}\neq 0$, it fails in satisfying the periodicity constraint for the integral $\int_0^L \varepsilon(X)\rho_0 \mathrm{d}X=0$ or in satisfying a sum-to-integral equivalence for the sum of squared strains (that is, for $\sum_{\alpha=1}^{N}\left(\varepsilon^{(\alpha)}\right)^2$), respectively. We want the strain field to always satisfy these equivalences. In order to correct it, we need to subtract a constant and add some roughness, that is, terms with small wavelengths. We come at the proposal of

$$\varepsilon(X)=\varepsilon^{\mathrm{F}}(X)-\hat{\varepsilon}^{(0)}+\hat{\varepsilon}^{(N/2)}\sin\left(\frac{\pi X}{a_0}\right) \tag{2.20}$$

as a final **regularization for the strain field** which is smoothest as possible and satisfies

$$\varepsilon(X^{(\alpha)})=\varepsilon^{(\alpha)},\quad \sum_{\alpha=1}^{N}\varepsilon^{(\alpha)}=\int_0^L \varepsilon(X)\rho_0\mathrm{d}X=0 \quad\text{and}\quad \sum_{\alpha=1}^{N}\left(\varepsilon^{(\alpha)}\right)^2=\int_0^L \varepsilon^2(X)\rho_0\mathrm{d}X, \tag{2.21}$$

where the last equation is a result of the Parseval's theorem.

For the sums of cubes or higher powers of $\varepsilon^{(\alpha)}$, equation (2.20) fails to provide general sum-to-integral equivalences. In order to also have these equivalences, some terms with smaller wavelengths should be used in the regularization (more specifically, terms of $\sin(m\pi X/a_0)$ with integer $m>1$). But then, with such fluctuations within small scales, the perturbative approximation of equation (2.15) would need more terms, with higher derivatives.

With the action of external forces $F^{\mathrm{ext},(\alpha)}$ at each particles and considering the displacement field obtained by integration of equation (2.20), we can assure

$$\sum_{\alpha=1}^{N}F^{\mathrm{ext},(\alpha)}u\left(X^{(\alpha)}\right)=\int_0^L F^{\mathrm{ext}}(X)u(X)\rho_0\mathrm{d}X. \tag{2.22}$$

if we make the following **regularization for the continuum external force field**

$$F^{\mathrm{ext}}(X)=F^{\mathrm{ext,F}}(X)-\hat{F}^{\mathrm{ext},(N/2)}\sin\left(\frac{\pi X}{a_0}\right), \tag{2.23}$$

where $F^{\mathrm{ext,F}}(X)=\sum_{n=1-N/2}^{N/2}\mathrm{Re}\left(\hat{F}^{\mathrm{ext},(n)}e^{i\frac{2\pi nX}{L}}\right)$ and $\hat{F}^{\mathrm{ext},(n)}=\frac{1}{N}\sum_{\alpha=1}^{N}F^{\mathrm{ext},(\alpha)}e^{-i\frac{2\pi n\alpha}{N}}$. In general, the physical setup of the system already provides a continuum function for the external force field, but only its values at the particles' positions will matter.

We then use these values as $F^{\text{ext},(\alpha)}$ and construct the regularized field of equation (2.23). At positions where there are no particles, it may be different from the one given by the system's setup.

When deriving a physical theory of elasticity, in the next chapter, we obtain that the energy is given by sums likes the ones in equations (2.21) and (2.22). Thus, we suppose that the discrete to continuum transitions are possible due to the existence of regularizations that assure us sum-to-integral equivalences. On the other hand, the resulted continuum theory can provide us equations to obtain the strain field for a given system. Thus, **the field resulted from theory must be "regularized back" in order to consistently predict both the discrete strain values and the energy**.

2.2 2D CRYSTALS

Now we turn to general 2D crystals, that is, without specifying the unit cell which is repeated.

2.2.1 Definition of displacement and strain fields in 2D

In 2D deformations, the positions $\{\mathbf{R}^{(\alpha)}\}$ of a perfect crystal displace to new positions $\{\mathbf{r}^{(\alpha)}\}$ by

$$\mathbf{u}^{(\alpha)} = \mathbf{r}^{(\alpha)} - \mathbf{R}^{(\alpha)}, \quad \text{or} \quad u_i^{(\alpha)} = r_i^{(\alpha)} - R_i^{(\alpha)}, \tag{2.24}$$

where we use latin subscripts to indicate cartesian components. From this we can define a displacement field $\mathbf{u}(\mathbf{R})$ which satisfies $\mathbf{u}(\mathbf{R}^{(\alpha)}) = \mathbf{u}^{(\alpha)}$. Here, there are four different displacement derivatives. In order to define discrete values for these derivatives, in the sense of equation (2.11), we use the tensor $\boldsymbol{\nabla}\mathbf{u}$ (or $\partial_i u_j$, in index form, where $\partial_i = \partial/\partial R_i$ in the Lagrangian description and $\partial_i = \partial/\partial r_i$ in the Eulerian one). We consider that it has discrete values which can be used to approximate

$$u_i^{(\beta,\alpha)} = u_i^{(\beta)} - u_i^{(\alpha)} \approx \big(R_j^{(\beta)} - R_j^{(\alpha)}\big)(\partial_j u_i)^{(\alpha)} = R_j^{(\beta,\alpha)}(\partial_j u_i)^{(\alpha)} \tag{2.25}$$

for all β neighbors of α, where we use the Einstein summation convention along this thesis (e.g., $A_{ijjk}B_{kl} = A_{ixxx}B_{xl} + A_{iyyx}B_{xl} + A_{ixxy}B_{yl} + A_{iyyy}B_{yl}$).

For each particle α, the best values of the components of $(\partial_i u_j)^{(\alpha)}$ can be obtained via least squares by minimizing the sum

$$\Omega\left((\partial_x u_x)^{(\alpha)}, (\partial_x u_y)^{(\alpha)}, (\partial_y u_x)^{(\alpha)}, (\partial_y u_y)^{(\alpha)}\right) = \sum_{\alpha^{\mathrm{nn}}} \left|\mathbf{u}^{(\alpha^{\mathrm{nn}},\alpha)} - \mathbf{R}^{(\bar{\alpha}^{\mathrm{nn}},\alpha)} \cdot (\boldsymbol{\nabla}\mathbf{u})^{(\alpha)}\right|^2 \quad (2.26)$$

over all particles α^{nn} that are nearest neighbors of α in the deformed crystal, where $\bar{\alpha}^{\mathrm{nn}} = \bar{\alpha}^{\mathrm{nn}}(\alpha^{\mathrm{nn}})$ associates each nearest neighbor in the deformed crystal with a nearest neighbor in the prefect one. Thus, **we can use the values of** $(\partial_i u_j)^{(\alpha)}$ **that minimize equation (2.26) as the discrete values which, in a continuum assumption, provide the continuum field** $\partial_i u_j(\mathbf{R})$. This is a 2D generalization of the second definition in equation (2.11). Here, additional care should be taken.

Figure 3 – Region of a triangular crystal which was deformed by a dislocation. The mean center of the dislocation is indicated by gray $\perp$ symbol. The lines represent bonds between nearest neighboring particles, which were defined via **Delaunay triangulation**. Black thin lines are bonds from the perfect crystal that continued to exist after deformation. Blue and red lines are bonds that were formed and broken, respectively. Yellow particles have lost or gained neighbors, while green particles have exchanged neighbors.

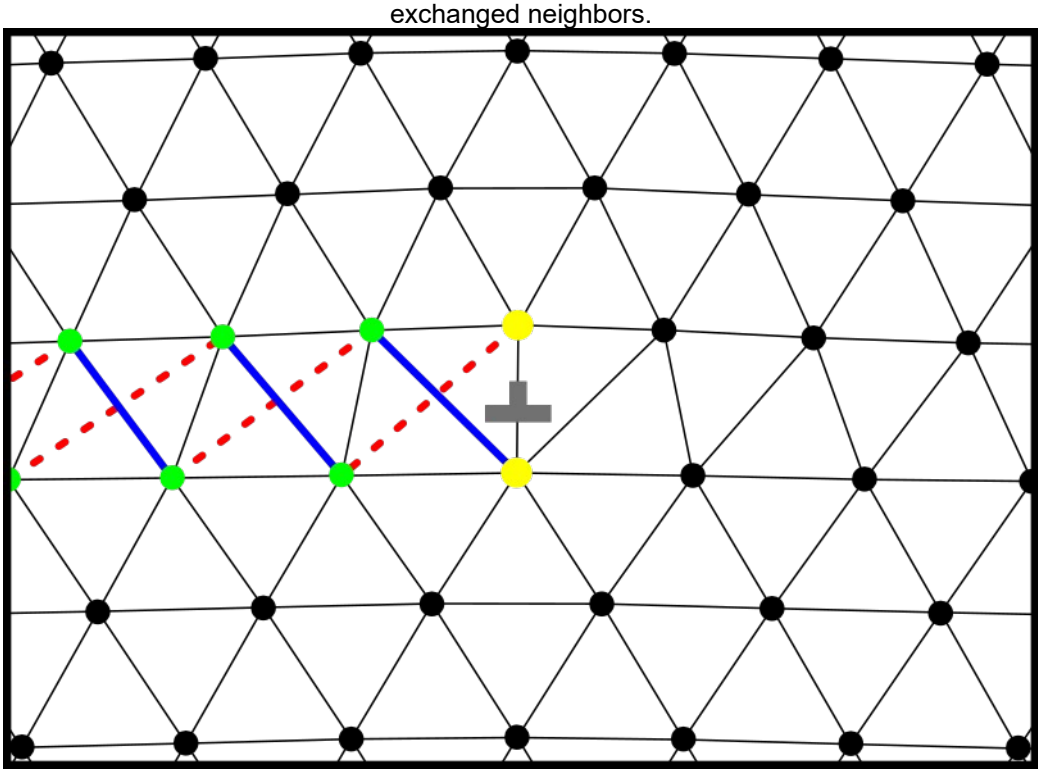

Source: The Author (2023).

Lets consider slip deformations, along slip lines of the crystal, and their beginnings and endings, which are called **dislocations**. In this case, particles exchange neighbors but maintains the same crystalline structure in most part of the crystal, except very near the dislocations. Lets also consider that each dislocation is far from others. Figure 3 shows such a system, zooming on a single dislocation.

In this case, along the slip line (formed by green particles), the displacement field has a great variation within a small distance. Nevertheless, such variation does no affect relevant physical quantities, such as energy and particle densities. Due to the reflection symmetry in figure 3, they are equal for particles on the left and on the right side of figure 3. We want the theory to respect such equivalence of these quantities while ignoring dependencies on higher derivatives of $\mathbf{u}$. One way to do so, in triangular crystals, is to **consider that the sum in equations (2.26) runs only through the neighbors α^{nn} that have themselves 6 nearest neighbors**. In other words, the particle α in equation (2.26) can be anyone, while the particles α^{nn} cannot include any of the yellow particles shown in figure 3. Moreover, the injection $\bar{\alpha}^{\mathrm{nn}}(\alpha^{\mathrm{nn}})$ to be used is the one that minimizes Ω further. Then the resulting values of $(\partial_i u_j)^{\alpha}$ respect the reflection symmetry in figure 3.

In the limit of small deformations, which is used in our thesis, the **strain tensor** is given by

$$\boldsymbol{\varepsilon} = \frac{\boldsymbol{\nabla}\mathbf{u} + (\boldsymbol{\nabla}\mathbf{u})^{\mathrm{T}}}{2} \qquad \text{or} \qquad \varepsilon_{ij} = \frac{\partial_i u_j + \partial_j u_i}{2}, \tag{2.27}$$

where $\boldsymbol{A}^{\mathrm{T}}$ is the transpose of $\boldsymbol{A}$ (i.e., $A^{\mathrm{T}}_{ij} = A_{ji}$). The antisymmetric combination of derivatives of $\mathbf{u}$ is neglected here since it does not strain the system. In fact, it is associated with rotations, as we show in the next subsection. Finally we can define discrete strain values $\varepsilon_{ij}^{(\alpha)}$ directly from the minimization of equation (2.26).

2.2.2 Types of homogeneous deformation

In order to know how each derivative of the displacement field deforms the system, lets consider the **deformation gradient tensor**

$$\boldsymbol{F} = \boldsymbol{I} + (\boldsymbol{\nabla}\mathbf{u})^{\mathrm{T}}, \tag{2.28}$$

where $\boldsymbol{I}$ is the identity matrix (i.e., δ_{ij}). This tensor tells how small line elements changed during deformation, since $\mathrm{d}\mathbf{r} = \boldsymbol{F} \cdot \mathrm{d}\mathbf{R}$. We can use the **singular value decomposition** to write

$$\boldsymbol{F} = \boldsymbol{R}^{\mathrm{P}}(\psi) \cdot \boldsymbol{R}^{\mathrm{P}}(\varphi) \cdot \begin{bmatrix} A_{\parallel} & 0 \\ 0 & A_{\perp} \end{bmatrix} \cdot \boldsymbol{R}^{\mathrm{P}}(-\varphi), \tag{2.29}$$

where $\boldsymbol{R}^{\mathrm{P}}(\theta) = \left[\begin{smallmatrix} \cos\theta & -\sin\theta \\ \sin\theta & \cos\theta \end{smallmatrix}\right]$ is the proper rotation matrix, ψ and φ are angles, $A_{\parallel}$ is the stretch in the direction of φ and $A_{\perp}$ is the stretch in the direction perpendicular to it.

The area element is changed by a factor of $A_{\parallel}A_{\perp}$ while

$$\delta\bar{\rho} = (\rho - \rho_0)/\rho_0 = (A_{\parallel}A_{\perp})^{-1} - 1 \tag{2.30}$$

is the **relative density variation**. A shape change happens if $A_{\parallel} \neq A_{\perp}$, indicating that a pure shear is applied. A convenient **shear quantifier** is

$$s = \ln(A_{\parallel}/A_{\perp}) \tag{2.31}$$

and such pure **shear is applied at the direction given by** φ. Moreover, note that ψ is the **net rotation**. In the limit of small deformations, $\delta\bar{\rho}$, s and ψ are small, while φ does not need to be. The deformation gradient tensor then becomes

$$\boldsymbol{F} = \frac{1}{\sqrt{1+\delta\bar{\rho}}}\begin{bmatrix}\cosh\left(\frac{s}{2}\right)\cos\psi + \sinh\left(\frac{s}{2}\right)\cos(2\varphi+\psi) & \sinh\left(\frac{s}{2}\right)\sin(2\varphi+\psi) - \cosh\left(\frac{s}{2}\right)\sin\psi \\ \sinh\left(\frac{s}{2}\right)\sin(2\varphi+\psi) + \cosh\left(\frac{s}{2}\right)\sin\psi & \cosh\left(\frac{s}{2}\right)\cos\psi - \sinh\left(\frac{s}{2}\right)\cos(2\varphi+\psi)\end{bmatrix} \tag{2.32}$$

$$\approx \frac{1}{2}\begin{bmatrix}2-\delta\bar{\rho}+s\cos(2\varphi) & s\sin(2\varphi)-2\psi \\ s\sin(2\varphi)+2\psi & 2-\delta\bar{\rho}-s\cos(2\varphi)\end{bmatrix} \tag{2.33}$$

from which we can obtain, by comparing with equation (2.28),

$$\varepsilon_{xx} = \partial_x u_x \approx \frac{-\delta\bar{\rho} + s\cos(2\varphi)}{2}, \tag{2.34}$$

$$\varepsilon_{yy} = \partial_y u_y \approx \frac{-\delta\bar{\rho} - s\cos(2\varphi)}{2}, \tag{2.35}$$

and

$$\varepsilon_{xy} = \varepsilon_{yx} = \frac{\partial_x u_y + \partial_y u_x}{2} \approx \frac{s\sin(2\varphi)}{2}, \tag{2.36}$$

while

$$\boldsymbol{\nabla} \wedge \mathbf{u} = \partial_x u_y - \partial_y u_x \approx 2\psi \tag{2.37}$$

and thus $\boldsymbol{\nabla} \wedge \mathbf{u}$ **does not strains the system** in the limit of small deformations.

2.2.3 An alternative mathematical formalism

When considering dislocations with arbitrary Burgers vector directions, which will be defined in the next subsection, the tensorial formalism which uses the strains ε_{ij} can be arduous. Here we use complex numbers operations to define two **convenient deformation fields,** $\widetilde{S}$ **and** $\widetilde{C}$, such that

$$\begin{aligned}\widetilde{S} &= S_1 + iS_2 \\ &= \widetilde{\nabla}\widetilde{u} = (\partial_x u_x - \partial_y u_y) + i(\partial_x u_y + \partial_y u_x) \approx s e^{i2\varphi}\end{aligned} \tag{2.38}$$

and

$$\begin{aligned}\widetilde{C} &= C_1 + iC_2 \\ &= \widetilde{\nabla}^*\widetilde{u} = (\partial_x u_x + \partial_y u_y) + i(\partial_x u_y - \partial_y u_x) \approx -\delta\bar{\rho} + i2\psi,\end{aligned} \tag{2.39}$$

where $\widetilde{\nabla} = \partial_x + i\partial_y$ and $\widetilde{u} = u_x + iu_y$ are complex representations of the vectors $\boldsymbol{\nabla}$ and $\mathbf{u}$, and $\widetilde{A}^*$ is the complex conjugate of $\widetilde{A}$. These fields have interesting mathematical and physical properties and meanings. $\widetilde{S}$ **describes pure shear deformations**, which are responsible for shape changes. $\widetilde{C}$ **is associated with conformal deformations**, that is, the ones which do not affects the shape of the crystal, such as relative density variations (given by $-C_1$) and rotations (given by $C_2/2$).

One can note that, due to their behavior under rotations, $\widetilde{C}$ **and** $\widetilde{S}$ **are not representations of true vectors**. In fact, under proper rotations, a true vector (i.e., spin-1) $\mathbf{A}$ transform as $\mathbf{A}' = \boldsymbol{R}^{\mathrm{P}}(\theta) \cdot \mathbf{A}$, which can be written as $\widetilde{A}' = e^{i\theta}\widetilde{A}$, while we have

$$\widetilde{S}' = \widetilde{\nabla}'\widetilde{u}' = \big(e^{i\theta}\widetilde{\nabla}\big)\big(e^{i\theta}\widetilde{u}\big) = e^{i2\theta}\widetilde{S} \quad \text{and} \quad \widetilde{C}' = \widetilde{\nabla}'^{*}\widetilde{u}' = \big(e^{i\theta}\widetilde{\nabla}\big)^{*}\big(e^{i\theta}\widetilde{u}\big) = \widetilde{C}. \quad (2.40)$$

This means that $\widetilde{C}$ and $\widetilde{S}$ are spin-0 and spin-2 fields, respectively. In fact, $C_1 \approx -\delta\bar{\rho}$ and $C_2 \approx 2\psi$ are scalar and pseudoscalar fields, respectively. On the other hand, it makes sense for the shear field to be a spin-2 field since a pure shear on a direction φ becomes the opposite if exerted on the direction $\varphi + \pi/2$, and is the same if exerted on the direction $\varphi + \pi$.

Considering that

$$\widetilde{\nabla}^*\widetilde{S} = \widetilde{\nabla}^*\widetilde{\nabla}\widetilde{u} = \big[\nabla^2 + i(\boldsymbol{\nabla}\wedge\boldsymbol{\nabla})\big]\widetilde{u} \quad \text{and} \quad \widetilde{\nabla}\widetilde{C} = \widetilde{\nabla}\widetilde{\nabla}^*\widetilde{u} = \big[\nabla^2 - i(\boldsymbol{\nabla}\wedge\boldsymbol{\nabla})\big]\widetilde{u}, \quad (2.41)$$

we define the (spin-1) **Burgers vector density**

$$\mathbf{B} = (\boldsymbol{\nabla}\wedge\boldsymbol{\nabla})\mathbf{u} = (\partial_x\partial_y - \partial_y\partial_x)\mathbf{u}, \quad (2.42)$$

which is nonzero only in the presence of topological defects and will be more discussed in the next subsection. We then arrive at the following **compatibility equation**

$$\widetilde{\nabla}^*\widetilde{S} - \widetilde{\nabla}\widetilde{C} = 2i\widetilde{B}. \quad (2.43)$$

We can use the **Green's function for the 2D Laplacian**, given by $G(\mathbf{r}-\mathbf{r}') = \ln|\mathbf{r}-\mathbf{r}'|/2\pi$ with $\nabla^2 G(\mathbf{r}-\mathbf{r}') = \delta(\mathbf{r}-\mathbf{r}')$ and $(\boldsymbol{\nabla}\wedge\boldsymbol{\nabla})G(\mathbf{r}-\mathbf{r}') = 0$, where $\delta(\mathbf{r})$ is the **Dirac delta function**, to obtain **regular solutions for inhomogeneous differential equations of** $\widetilde{\nabla}\widetilde{A}$ **and** $\widetilde{\nabla}^*\widetilde{A}$, given by

$$\begin{aligned}\widetilde{A}(\mathbf{r}) &= \widetilde{\nabla}^* \int \big[\widetilde{\nabla}\widetilde{A}\big](\mathbf{r}')\; G(\mathbf{r}-\mathbf{r}')\; \mathrm{d}^2 r' + \widetilde{A}^{\mathrm{bc}}(\mathbf{r}) \\ &= \int \big[\widetilde{\nabla}\widetilde{A}\big](\mathbf{r}')\; \widetilde{\nabla}^* G(\mathbf{r}-\mathbf{r}')\; \mathrm{d}^2 r' + \widetilde{A}^{\mathrm{bc}}(\mathbf{r}) \end{aligned} \quad (2.44)$$

$$= \int \left[\widetilde{\nabla}\widetilde{A}\right](\mathbf{r}') \, \frac{(\widetilde{r} - \widetilde{r}')^*}{2\pi|\mathbf{r} - \mathbf{r}'|^2} \, \mathrm{d}^2 r' + \widetilde{A}^{\mathrm{bc}}(\mathbf{r}) \tag{2.45}$$

and

$$\widetilde{A}(\mathbf{r}) = \widetilde{\nabla} \int \left[\widetilde{\nabla}^* \widetilde{A}\right](\mathbf{r}') \, G(\mathbf{r} - \mathbf{r}') \, \mathrm{d}^2 r' + \widetilde{A}^{\mathrm{bc}}(\mathbf{r})$$

$$= \int \left[\widetilde{\nabla}^* \widetilde{A}\right](\mathbf{r}') \, \widetilde{\nabla} G(\mathbf{r} - \mathbf{r}') \, \mathrm{d}^2 r' + \widetilde{A}^{\mathrm{bc}}(\mathbf{r}) \tag{2.46}$$

$$= \int \left[\widetilde{\nabla}^* \widetilde{A}\right](\mathbf{r}') \, \frac{(\widetilde{r} - \widetilde{r}')}{2\pi|\mathbf{r} - \mathbf{r}'|^2} \, \mathrm{d}^2 r' + \widetilde{A}^{\mathrm{bc}}(\mathbf{r}), \tag{2.47}$$

respectively, where $\widetilde{A}^{\mathrm{bc}}$ is solution to the respective homogeneous equation such that the total field satisfy the boundary conditions. Since the **superposition principle** is valid in Linear Elasticity, we can analyze the deformation contribution due to the boundary conditions separately from the ones due to defects, external forces, etc.

When $\mathbf{B}$ and the boundary conditions are known, equation (2.43) gives $\widetilde{S}$ from (nonlocal values of) $\widetilde{C}$ and vice versa, by making use of equations (2.47) and (2.45), respectively. We can then entirely describe the deformation using only shape variations (i.e., shear deformations, described by $\widetilde{S}$) or, alternatively, using only variations in density and orientation (i.e., conformal deformations, described by $\widetilde{C}$). This shear-conformal duality originates from the mathematical duality between $\widetilde{C}$ and $\widetilde{S}$. As we will see in the next chapter, only the $\widetilde{C}$-picture can provide a local form of the field equations of Elasticity. On the other hand, only the $\widetilde{S}$-picture can provide a local form of the Peach-Koehler force.

2.3 THE BURGERS VECTOR OF A DISLOCATION

In 2D and higher dimensions there can appear deformations which cannot be undeformed locally. These are topological defects and one example is the dislocation, main object of analysis in this thesis. Figure 4 shows a perfect triangular crystal in (a) and a triangular crystal with a dislocation in (b). The topological charge of the dislocation can be obtained by observing what happens along a circuit around it.

Consider a set of distance vectors $\{\Delta\mathbf{R}^{(n)}\}$ connecting N^{circ} neighboring particles such that they closes a circuit, called **Burgers circuit** in the prefect crystal. The particles in the circuit are labeled by n and ordered along it, such that $\Delta\mathbf{R}^{(n)} = \mathbf{R}^{(n+1)} - \mathbf{R}^{(n)}$ and $\mathbf{R}^{(N^{\mathrm{circ}}+1)} = \mathbf{R}^{(1)}$, which gives $\sum_{n=1}^{N^{\mathrm{circ}}} \Delta\mathbf{R}^{(n)} = \mathbf{R}^{(N^{\mathrm{circ}}+1)} - \mathbf{R}^{(1)} = 0$

$\sum_{n=1}^{N^{\mathrm{circ}}} \Delta\mathbf{R}^{(n)} = \mathbf{R}^{(N^{\mathrm{circ}}+1)} - \mathbf{R}^{(1)} = 0$. Two examples of circuits like this are illustrated by the sets of green and blue arrows in figure 4(a).

Figure 4 – A perfect triangular crystal and a deformed one, with a dislocation in the center. The arrows indicate the Burgers circuits, as discussed in the text.

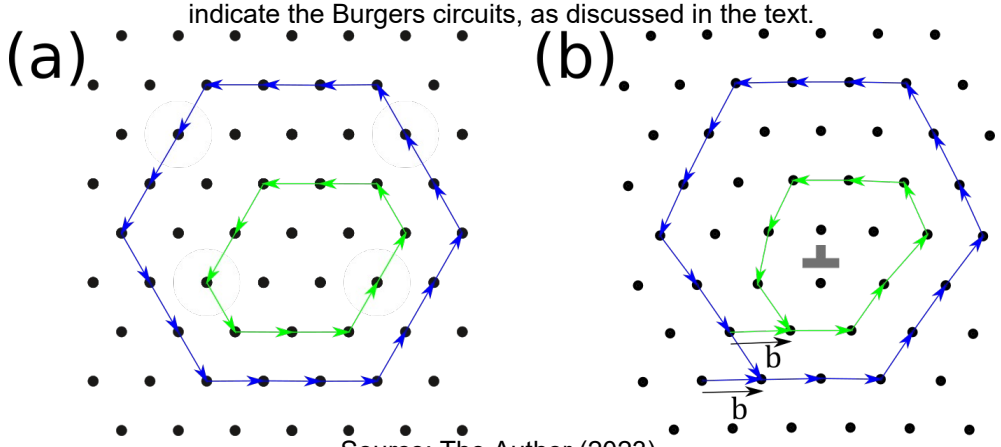

Source: The Author (2023).

In the same way, the respective distances $\{\Delta\mathbf{r}^{(n)}\}$ in the deformed crystal respects $\sum_{n=1}^{N^{\mathrm{circ}}} \Delta\mathbf{r}^{(n)} = \mathbf{r}^{(N^{\mathrm{circ}}+1)} - \mathbf{r}^{(1)} = 0$. However, it turns out that the theoretical distances $\{\Delta\bar{\mathbf{r}}^{(n)}\}$ predicted by the continuum deformation gradient tensor (that is, $\Delta\bar{r}_i^{(n)} = F_{ij}^{(n)}\Delta R_j^{(n)} = \left[\delta_{ij} + (\partial_j u_i)^{(n)}\right]\Delta R_j^{(n)}$), which are shown by the sets of green and blue arrows in figure 4(b), give $\sum_{n=1}^{N^{\mathrm{circ}}} \Delta\bar{\mathbf{r}}^{(n)} = \mathbf{b}$. This is due to the fact that the dislocation presence introduces a slip which starts (or ends) in it, while the values of $(\partial_i u_j)^{(\alpha)}$ taken from equation (2.26) ignore the effect of such slip. Thus, we can define the **Burgers vector**

$$\mathbf{b} \approx \sum_n \left(\Delta\bar{\mathbf{r}}^{(n)} - \Delta\mathbf{R}^{(n)}\right) = \sum_n \Delta\mathbf{R}^{(n)} \cdot \left(\boldsymbol{\nabla}\mathbf{u}\right)^{(n)} \approx \oint \mathrm{d}\mathbf{R} \cdot \boldsymbol{\nabla}\mathbf{u} \approx \oint \mathrm{d}\mathbf{r} \cdot \boldsymbol{\nabla}\mathbf{u} \qquad (2.48)$$

for any counterclockwise closed curve enclosing the dislocation and no other defect.

The first approximating step in equation (2.48) considers that $\mathbf{b}$ **is approximately the same for any circuit** around the dislocation. The **sum-to-integral transition here is generally approximate but not exact**, since the regularization for the continuum $\boldsymbol{\nabla}\mathbf{u}$ may assure the sum-to-integral equivalence for integrals over the whole system but cannot guarantee the equivalence for any finite line integral. The last approximation in equation (2.48) considers the **limit of small deformations**, in which the Langrangian and Eulerian descriptions are the same.

From vector calculus theorems, we can write $\oint \mathrm{d}\mathbf{r} \cdot \boldsymbol{\nabla}\mathbf{u}$ as $\oint \mathrm{d}\mathbf{u}$ or as $\int \mathrm{d}^2 r (\boldsymbol{\nabla} \wedge \boldsymbol{\nabla})\mathbf{u}$, which show that the displacement field in the presence of a

dislocation is multivalued and its derivatives do not commute. In fact, as the integral keeps the same while we decrease the integral region/curve as long as the dislocation is inside, then we have that the derivatives of $\mathbf{u}$ would commute everywhere except at the dislocation position. This means that, in a system with dislocations $\{\mathbf{b}^{(i)}\}$ located at $\{\mathbf{r}^{(i)}\}$, the Burgers vector density is given by

$$\mathbf{B}(\mathbf{r}) = \big(\boldsymbol{\nabla}\wedge\boldsymbol{\nabla}\big)\mathbf{u}(\mathbf{r}) = \sum_i \mathbf{b}^{(i)}\delta(\mathbf{r}-\mathbf{r}^{(i)}). \tag{2.49}$$

In fact, equation (2.49) is a continuum theory description for the Burgers vector density of **classically idealized point dislocations**. One way to define $\mathbf{B}$ from the discrete crystal configuration is to evaluate the discrete values of $\big(\partial_i u_j\big)^{(\alpha)}$ from minimization of equation (2.26), make a continuum assumption and take derivatives to obtain $B_i = \epsilon_{jk}\partial_j\partial_k u_i$. The result gives a nonlocalized Burgers vector density, which makes sense since the sum in equation (2.48) has a litte dependence on the circuit chosen. Continuum theory descriptions of the dislocation having a structure will be discussed in chapter 7.

Finally, we can **separate the displacement field into a regular part and a multivalued singular one**, such that

$$\nabla^2\widetilde{u}^{\mathrm{reg}} = \widetilde{\nabla}^*\widetilde{S}^{\mathrm{reg}} = \widetilde{\nabla}\widetilde{S}^{\mathrm{reg}}, \qquad \nabla^2\widetilde{u}^{\mathrm{sing}} = 0 \qquad \text{and} \qquad \big(\boldsymbol{\nabla}\wedge\boldsymbol{\nabla}\big)\widetilde{u}^{\mathrm{sing}} = \widetilde{B}. \tag{2.50}$$

For the case of just a point dislocation $\mathbf{b}$ located at the origin, the displacement field has a singular part which obeys $\big(\boldsymbol{\nabla}\wedge\boldsymbol{\nabla}\big)\mathbf{u}^{\mathrm{sing}} = \mathbf{b}\ \delta(\mathbf{r})$. In this case, we use equations (2.50), (2.47) and (2.45) to obtain

$$\widetilde{S}^{\mathrm{sing}}(\mathbf{r}) = \frac{i\,\widetilde{b}\,\widetilde{\hat{r}}}{2\pi|\mathbf{r}|} \qquad \text{and} \qquad \widetilde{C}^{\mathrm{sing}}(\mathbf{r}) = -\frac{i\,\widetilde{b}\,\widetilde{\hat{r}}^*}{2\pi|\mathbf{r}|} \tag{2.51}$$

where $\hat{\mathbf{r}} = \mathbf{r}/|\mathbf{r}|$. From $\oint \mathrm{d}\mathbf{u}^{\mathrm{sing}} = \mathbf{b}$, we have

$$\widetilde{u}^{\mathrm{sing}}(\mathbf{r}) = \frac{\widetilde{b}\arg(\widetilde{r})}{2\pi}, \tag{2.52}$$

where $\arg(z)$ is the argument of z, that is, $\arg(\widetilde{r})$ is the angle of the vector $\mathbf{r}$ with respect to the $\hat{\mathbf{x}}$-direction. In the next chapter, we will see that regular parts of the deformation fields are needed for them to satisfy the equilibrium equations of Classical Elasticity.

3 ELASTIC ENERGY AND SOME EXACT RESULTS OF CLASSICAL ELASTICITY

This chapter introduces the physics of elasticity for 2D crystals within some approximations that are classically taken. Moreover, we obtain exact results about the dislocation within Classical Elasticity Theory.

3.1 EQUILIBRIUM EQUATIONS OF CLASSICAL ELASTICITY

Under some conditions, the total potential energy variation due to a deformation in a crystal can be well approximated by a simple functional of the displacement field.

3.1.1 Classical pairwise interactions' contribution to the energy

In the present thesis, we consider classical identical particles interacting via a soft pairwise isotropic potential V, such that the **interaction potential energy** is

$$U^{\mathrm{int}}(\{\mathbf{r}^{(\alpha)}\}) = \sum_{\beta>\alpha} V\big(\mathbf{r}^{(\beta)}, \mathbf{r}^{(\alpha)}\big) = \sum_{\beta>\alpha} V\big(r^{(\beta,\alpha)}\big) = \frac{1}{2}\sum_{\alpha}\sum_{\beta\neq\alpha} V\big(r^{(\beta,\alpha)}\big), \tag{3.1}$$

where $r^{(\beta,\alpha)} = |\mathbf{r}^{(\beta,\alpha)}| = |\mathbf{r}^{(\beta)} - \mathbf{r}^{(\alpha)}|$ and the "$1/2$" in the last passage appears because each pair is being counted twice. Considering that the system is infinite, with a fixed density, the configuration of minimum energy is crystalline for most potentials V of interest. Thus, the lattice sum

$$\Phi = \sum_{\beta\neq\alpha} V\big(r^{(\beta,\alpha)}\big) \tag{3.2}$$

on β, sometimes called the **Madelung energy**, is usually the same for every particle and depends on the crystal's density and structure.

In chapter 5, we simulate a system with $V(r) = U_0(\sigma_0/r)^{12}$, which forms a triangular crystal at zero temperature. The Madelung energy in this case, is calculated to be

$$\Phi = \Lambda_{12} U_0 \left(\frac{\sigma_0}{a_0}\right)^{12}, \tag{3.3}$$

where a_0 is the distance between neighbors and $\Lambda_{12} \approx 6.00981$ is obtained by summing $1/(n^2+m^2+nm)^6$ over all integer values of n and m except when both are zero.

3.1.2 Approximations for smooth and small deformations

For short ranged interactions, such as the one that we will use in our simulations, only the pairs of nearby particles provide non-negligible terms in the interaction energy (equation (3.1)). For such pairs, we can use the **smooth deformation approximation** of equation (2.25)

$$r_i^{(\beta,\alpha)} = R_i^{(\beta,\alpha)} + u_i^{(\beta,\alpha)} \approx \left[\delta_{ij} + (\partial_j u_i)^{(\alpha)}\right] R_j^{(\beta,\alpha)}, \tag{3.4}$$

where the values of $(\partial_i u_j)^{(\alpha)}$ are ones that minimize equation (2.26). Here, in fact, we used only the first term of the expansion in equation (2.15), neglecting terms with derivatives of strains. Specifically, we are considering that the n-th order derivatives of $\partial_i u_j$ are much smaller than $(\partial_i u_j)^{(\alpha)}/a_0^n$.

Moreover, we use the **small deformation approximation** that considers $(\partial_i u_j)^{(\alpha)} \ll 1$ to perform expansions up to second order in these quantities. Then we obtain

$$V\left(r^{(\beta,\alpha)}\right) \approx V\left(R^{(\beta,\alpha)}\right) + J_{ij}^{(\beta,\alpha)} (\partial_i u_j)^{(\alpha)} + C_{ijkl}^{(\beta,\alpha)} (\partial_i u_j)^{(\alpha)} (\partial_k u_l)^{(\alpha)}, \tag{3.5}$$

where the coefficients depend only on distances in the perfect crystal and are given by

$$J_{ij}^{(\beta,\alpha)} = \frac{R^{(\beta,\alpha)} V'\left(R^{(\beta,\alpha)}\right)}{2} \hat{R}_i^{(\beta,\alpha)} \hat{R}_j^{(\beta,\alpha)} \tag{3.6}$$

and

$$C_{ijkl}^{(\beta,\alpha)} = \frac{R^{(\beta,\alpha)}}{2} \left[\frac{\left[R^{(\beta,\alpha)} V''\left(R^{(\beta,\alpha)}\right) - V'\left(R^{(\beta,\alpha)}\right)\right]}{4} \hat{R}_k^{(\beta,\alpha)} \hat{R}_l^{(\beta,\alpha)} + V'\left(R^{(\beta,\alpha)}\right) \delta_{kl} \right] \hat{R}_i^{(\beta,\alpha)} \hat{R}_j^{(\beta,\alpha)}, \tag{3.7}$$

where $\hat{R}_i^{(\beta,\alpha)} = R_i^{(\beta,\alpha)}/R^{(\beta,\alpha)}$ and the primes indicate derivatives.

3.1.3 Elastic interaction energy and the continuum assumption

We will consider that the system is under PBC, in which a rectangular box with sizes L_x and L_y and with N particles is infinitely repeated. In this case, the particles near the boundaries interact with the image particles. Note that Fourier series and a regularization like the one of equation (2.20) can also be used here.

As the PBC simulates an infinite system, by using the approximation of equation (3.5) in the interaction energy given by equation (3.1), we can omit the sum in β. In crystals such as the triangular one, symmetry gives us the constants

$$J_{ij} = \rho_0 \sum_{\beta \neq \alpha} J_{ij}^{(\beta,\alpha)} \qquad \text{and} \qquad C_{ijkl} = \rho_0 \sum_{\beta \neq \alpha} C_{ijkl}^{(\beta,\alpha)}, \tag{3.8}$$

where the undeformed crystal's density ρ_0, which is $2/\sqrt{3}a_0^2$ for triangular crystals, was introduced here for convenience. Now, we can use equation (3.1), (3.5), (3.12), (3.13) and (3.8) to obtain the **total interaction energy due to elastic deformations**, which is given by

$$\begin{aligned}
\Delta U^{\text{int}} &= U^{\text{int}}(\{\mathbf{r}^{(\alpha)}\}) - U^{\text{int}}(\{\mathbf{R}^{(\alpha)}\}) \\
&\approx \frac{1}{2\rho_0} \sum_{\alpha} \left[J_{ij} (\partial_i u_j)^{(\alpha)} + C_{ijkl} (\partial_i u_j)^{(\alpha)} (\partial_k u_l)^{(\alpha)} \right] && (3.9) \\
&= \frac{1}{2} \int \left[J_{ij} \partial_i u_j(\mathbf{R}) + C_{ijkl} \partial_i u_j(\mathbf{R}) \partial_k u_l(\mathbf{R}) \right] \mathrm{d}^2 R && (3.10) \\
&= \frac{1}{2} \int C_{ijkl} \partial_i u_j(\mathbf{R}) \partial_k u_l(\mathbf{R}) \mathrm{d}^2 R, && (3.11)
\end{aligned}$$

where the sum is performed over the particles inside the box of PBC, the integral is performed over the box area, the sum-to-integral equivalence is guaranteed by a regularization like the one of equation (2.20) and the integral of $\partial_i u_j(\mathbf{R})$ is zero due to the PBC.

3.1.4 Conservative external potential and additional approximations

In the presence of a conservative external potential field $V^{\text{ext}}(\mathbf{r})$, we have the following **external potential energy** contribution to the total energy

$$U^{\text{ext}}(\{\mathbf{r}^{(\alpha)}\}) = \sum_{\alpha} V^{\text{ext}}(\mathbf{r}^{(\alpha)}). \tag{3.12}$$

We consider that V^{ext} respects the periodicity of the PBC and has a Fourier series whose terms have wavelengths larger or equal to 2π divided by the minimum distance of the crystal's periodicity in the respective direction (e.g., the triangular lattice shown in figure 4(a) has periodicity a_0 in the $\hat{\mathbf{x}}$-direction and $\sqrt{3}a_0/2$ in the $\hat{\mathbf{y}}$-direction).

Considering also a **small displacement approximation**, where the values of $u_i^{(\alpha)}$ are much smaller than the minimum wavelength of the Fourier series of V^{ext}, we can approximate

$$V^{\text{ext}}(\mathbf{r}^{(\alpha)}) \approx V^{\text{ext}}(\mathbf{R}^{(\alpha)}) - F_i^{\text{ext}}(\mathbf{R}^{(\alpha)}) u_i^{(\alpha)}, \tag{3.13}$$

where $\mathbf{F}^{\text{ext}} = -\boldsymbol{\nabla} V^{\text{ext}}$ is the external body force field. In fact, we are considering that the external forces on the particles are small in such a way that the displacements due to it are small.

Now we consider the **continuum approximation**

$$\mathbf{u}^{(\alpha)} \approx \mathbf{u}(\mathbf{R}^{(\alpha)}). \tag{3.14}$$

This is not exact since the continuum field $\mathbf{u}(\mathbf{R})$ we are considering here is the one obtained by integration of the continuum fields $\partial_i u_j(\mathbf{R})$ considered in the previous subsection. The four derivative fields $\partial_i u_j$ can provide not only a regular field $\mathbf{u}$ but also a singular one if the corresponding $\mathbf{B}$, given by equation (2.43), is nonzero.

For **total external potential energy due to elastic deformations**, we have

$$\begin{aligned} \Delta U^{\text{ext}} &= U^{\text{ext}}(\{\mathbf{r}^{(\alpha)}\}) - U^{\text{ext}}(\{\mathbf{R}^{(\alpha)}\}) \\ &\approx -\sum_{\alpha} F_i^{\text{ext}}\big(\mathbf{R}^{(\alpha)}\big) u_i(\mathbf{R}^{(\alpha)}) \qquad (3.15) \\ &= -\int f_i^{\text{ext}}\big(\mathbf{R}\big) u_i\big(\mathbf{R}\big) \mathrm{d}^2 R, \qquad (3.16) \end{aligned}$$

where $f_i^{\text{ext}} = \rho_0 F_i^{\text{ext}}$ and the sum-to-integral equivalence is guaranteed in the same way as equation (2.22) is.

3.1.5 Classical Elasticity Equations in the limit of zero temperature

For the approximations we have made, the **total elastic potential energy** is the following functional of the displacement field

$$\begin{aligned} E^{\text{el}}[\mathbf{u}] &= \Delta U^{\text{int}}[\mathbf{u}] + \Delta U^{\text{ext}}[\mathbf{u}] \\ &\approx \int \left[\frac{1}{2} C_{ijkl} \partial_i u_j\big(\mathbf{R}\big) \partial_k u_l\big(\mathbf{R}\big) - f_i^{\text{ext}}\big(\mathbf{R}\big) u_i\big(\mathbf{R}\big)\right] \mathrm{d}^2 R, \end{aligned} \tag{3.17}$$

which provides the following equilibrium equation

$$\frac{\delta E^{\text{el}}[\mathbf{u}]}{\delta u_i} = 0 \quad \Longrightarrow \quad C_{ijkl} \partial_i \partial_k u_l + f_j^{\text{ext}} = 0. \tag{3.18}$$

We call **Classical Elasticity** for equilibrium the theory that uses the previous equation together with the compatibility equation

$$\epsilon_{jk} \partial_j \partial_k u_i = B_i, \tag{3.19}$$

where ϵ_{jk} and B_i are the **Levi-Civita symbol** $\boldsymbol{\epsilon} = \left[\begin{smallmatrix} 0 & 1 \\ -1 & 0 \end{smallmatrix}\right]$ and the Burgers vector density $\mathbf{B}$ in index form.

By ignoring the kinetic energy and minimizing the potential one, the **limit of zero temperature** is being considered for the Classical Elasticity equations above.

The linearity of them allows the use of the superposition principle. Moreover, while using such continuum theory, it is usual to impose no restrictions of regularization for the displacements and strain fields. As commented in section 2.1.5, this can lead to problems when there are fluctuations within scales of a_0 or smaller.

Finally, we remark that the Classical Elasticity has the same form in the Eulerian description. We are considering that $\partial_i u_j$, f_i and u_i are small quantities. Therefore, in the passage from an integral in $\mathbf{R}$ to an integral in $\mathbf{r}$, we use the Jacobian determinant

$$\det\left|\boldsymbol{\nabla}\mathbf{R}\right| = \frac{1}{2}\epsilon_{lj}\epsilon_{ki}\partial_l R_k \partial_j R_i = 1 - \partial_i u_i + \frac{1}{2}\epsilon_{lj}\epsilon_{ki}\partial_l u_k \partial_j u_i, \tag{3.20}$$

where the derivatives here are with respect to $\mathbf{r}$, and the energy up to second order in small quantities continues the same, that is,

$$E^{\mathrm{el}}[\mathbf{u}] \approx \int \left[\frac{1}{2}C_{ijkl}\partial_i u_j(\mathbf{r})\partial_k u_l(\mathbf{r}) - f_i^{\mathrm{ext}}(\mathbf{r})u_i(\mathbf{r})\right] \mathrm{d}^2 r. \tag{3.21}$$

For many crystals, such as the triangular one, the elastic constants satisfy the symmetry $C_{ijkl} = C_{jikl} = C_{ijlk}$. Using this to symmetrize $\partial_i u_j$, performing integration by parts in the external force term and using the divergence theorem, we can write the energy as

$$E^{\mathrm{el}}[\mathbf{u}] \approx \int \left[\frac{1}{2}C_{ijkl}\varepsilon_{ij}(\mathbf{r})\varepsilon_{kl}(\mathbf{r}) + V^{\mathrm{ext}}(\mathbf{r})\varepsilon_{ii}(\mathbf{r})\right] \mathrm{d}^2 r. \tag{3.22}$$

3.2 EXACT RESULTS FOR THE DISLOCATION IN CLASSICAL ELASTICITY

3.2.1 The Peach-Koehler force on a dislocation

In order to obtain the force on a dislocation, we will evaluate the total energy variation of the system due to a small variation of the dislocation position. In order to do so, we use the fact that the Classical Elasticity equations obey the superposition principle to separate the displacement field into one due to the dislocation and one due to the background, i.e., $\mathbf{u} = \mathbf{u}^{\mathrm{d}} + \mathbf{u}^{\mathrm{bg}}$.

The background field satisfies the equilibrium condition

$$C_{ijkl}\partial_i\partial_k u_l^{\mathrm{bg}} + f_j^{\mathrm{ext}} = 0. \tag{3.23}$$

The dislocation field has, in turn, singular and regular parts. The singular one is responsible for

$$\epsilon_{jk}\partial_j\partial_k u_i^{\mathrm{d}} = b_i\delta(\mathbf{r}-\mathbf{r}^{\mathrm{d}}), \tag{3.24}$$

where $\mathbf{r}^{\mathrm{d}}$ is the dislocation position. A regular part is needed for the dislocation to be in equilibrium with the crystal, i.e., to satisfy

$$C_{ijkl}\partial_i\partial_k u_l^{\mathrm{d}} = 0. \tag{3.25}$$

From the previous equations and considering a variation $\delta\mathbf{r}^{\mathrm{d}}$ in the dislocation position we have that

$$u_j^{\mathrm{d}} = u_j^{\mathrm{d}}(\mathbf{r}-\mathbf{r}^{\mathrm{d}}) \quad \Longrightarrow \quad \delta u_j^{\mathrm{d}} = -\delta r_n^{\mathrm{d}}\partial_n u_j^{\mathrm{d}} \quad \text{and} \quad \delta(\partial_i u_j^{\mathrm{d}}) = -\delta r_n^{\mathrm{d}}\partial_n\partial_i u_j^{\mathrm{d}}, \tag{3.26}$$

while $\delta u_j^{\mathrm{bg}} = 0$.

Finally, $\delta\mathbf{r}^{\mathrm{d}}$ varies the total elastic energy of interaction between the dislocation and the background by

$$\delta E^{\mathrm{d-bg}} = \int\Big[C_{ijkl}\partial_k u_l^{\mathrm{bg}}\delta(\partial_i u_j^{\mathrm{d}}) - f_j^{\mathrm{ext}}\delta u_j^{\mathrm{d}}\Big]\mathrm{d}^2 r \tag{3.27}$$

$$= -\int\Big[C_{ijkl}\partial_k u_l^{\mathrm{bg}}\partial_n\partial_i u_j^{\mathrm{d}} - f_j^{\mathrm{ext}}\partial_n u_j^{\mathrm{d}}\Big]\delta r_n^{\mathrm{d}}\ \mathrm{d}^2 r \tag{3.28}$$

$$= -\int\Big[C_{ijkl}\partial_k u_l^{\mathrm{bg}}(\partial_n\partial_i u_j^{\mathrm{d}} - \partial_i\partial_n u_j^{\mathrm{d}}) + C_{ijkl}\partial_k u_l^{\mathrm{bg}}\partial_i\partial_n u_j^{\mathrm{d}} - f_j^{\mathrm{ext}}\partial_n u_j^{\mathrm{d}}\Big]\delta r_n^{\mathrm{d}}\ \mathrm{d}^2 r. \tag{3.29}$$

Now, using integration by parts, the divergence theorem, the identity $(\partial_n\partial_i - \partial_i\partial_n) = \epsilon_{ni}\epsilon_{mp}\partial_m\partial_p$ and equations (3.23) and (3.24), we find

$$\begin{aligned}\delta E^{\mathrm{d-bg}} &= -\int\Big[C_{ijkl}\partial_k u_l^{\mathrm{bg}}\epsilon_{ni}\epsilon_{mp}\partial_m\partial_p u_j^{\mathrm{d}} - (C_{ijkl}\partial_i\partial_k u_l^{\mathrm{bg}} + f_j^{\mathrm{ext}})\partial_n u_j^{\mathrm{d}}\Big]\,\delta r_n^{\mathrm{d}}\ \mathrm{d}^2 r \\ &= -\int C_{ijkl}\partial_k u_l^{\mathrm{bg}}(\mathbf{r})\epsilon_{ni}b_j\delta(\mathbf{r}-\mathbf{r}^{\mathrm{d}})\delta r_n^{\mathrm{d}}\ \mathrm{d}^2 r \\ &= -C_{ijkl}\partial_k u_l^{\mathrm{bg}}(\mathbf{r}^{\mathrm{d}})\epsilon_{ni}b_j\delta r_n^{\mathrm{d}}.\end{aligned} \tag{3.30}$$

Therefore, within Classical Elasticity, the force on a dislocation due to the background is given by

$$f_n^{\mathrm{PK}} = -\frac{\delta E^{\mathrm{d-bg}}}{\delta r_n^{\mathrm{d}}} = \epsilon_{ni}b_j C_{ijkl}\partial_k u_l^{\mathrm{bg}}(\mathbf{r}^{\mathrm{d}}) \tag{3.31}$$

and is called the **Peach-Koehler force**.

3.2.2 Conservation of the particle number and dislocation glide

In any change of the system which does not add or remove a particle, such as a dislocation movement, the total number of particles must be conserved. This number can be defined within Classical Elasticity by using the Jacobian determinant as a relative density function, giving

$$N[\mathbf{u}] = \rho_0 \int \det\left|\boldsymbol{\nabla}\mathbf{R}\right| \mathrm{d}^2 r = \rho_0 \int \left[1 - \partial_i u_i(\mathbf{r}) + \frac{1}{2}\epsilon_{lj}\epsilon_{ki}\partial_l u_k(\mathbf{r})\partial_j u_i(\mathbf{r})\right] \mathrm{d}^2 r. \quad (3.32)$$

With a variation $\delta\mathbf{r}^{\mathrm{d}}$ of the dislocation position, the number of particles varies as

$$\delta N = \rho_0 \int \left[-\delta(\partial_i u_i^{\mathrm{d}}) + \epsilon_{lj}\epsilon_{ki}\partial_l u_k^{\mathrm{d}} \delta(\partial_j u_i^{\mathrm{d}})\right] \mathrm{d}^2 r \quad (3.33)$$

$$= \rho_0 \int \left[\partial_n \partial_i u_i^{\mathrm{d}} - \epsilon_{lj}\epsilon_{ki}\partial_l u_k^{\mathrm{d}} \partial_n \partial_j u_i^{\mathrm{d}}\right] \delta r_n^{\mathrm{d}} \ \mathrm{d}^2 r. \quad (3.34)$$

Now, using $\partial_n \partial_j u_i^{\mathrm{d}} = \partial_j \partial_n u_i^{\mathrm{d}} + \epsilon_{nj} b_i \delta(\mathbf{r} - \mathbf{r}^{\mathrm{d}})$, the divergence theorem and integration by parts, we find

$$\delta N = \rho_0 \int b_i \delta(\mathbf{r} - \mathbf{r}^{\mathrm{d}}) \left[\epsilon_{ni} + (\epsilon_{in}\partial_j + \epsilon_{nj}\partial_i + \epsilon_{ji}\partial_n) u_j^{\mathrm{d}}\right] \delta r_n^{\mathrm{d}} \ \mathrm{d}^2 r \quad (3.35)$$

$$= \rho_0 \delta r_n^{\mathrm{d}} \epsilon_{ni} b_i = \rho_0 \delta\mathbf{r}^{\mathrm{d}} \wedge \mathbf{b}, \quad (3.36)$$

where we used the identity $\epsilon_{in}A_j + \epsilon_{nj}A_i + \epsilon_{ji}A_n = 0$. When $\delta\mathbf{r}^{\mathrm{d}} \parallel \mathbf{b}$, we call it a dislocation glide. The continuum theory of Classical Elasticity gives that the glide is the unique movement that preserves N, unless another dislocation moves at the same time in order to counterbalance δN. For this reason, the glide is the most ubiquitous type of dislocation movement and it is the one that we focus on the present thesis.

3.2.3 Triangular crystal, $\widetilde{S}$- and $\widetilde{C}$-formalism and conformal crystals

Lets make explicit the equations of Classical Elasticity for a triangular crystal. The symmetry of such crystal provides $C_{ijkl} = B\delta_{ij}\delta_{kl} + \mu(\delta_{ik}\delta_{jl} + \delta_{il}\delta_{jk} - \delta_{ij}\delta_{kl})$, where B and μ are the bulk and shear moduli, respectively. Using this in the elastic energy functional, we obtain the following expression using the formalism introduced in section 2.2.3

$$E^{\mathrm{el}} = \frac{1}{2}\int \left[BC_1^2(\mathbf{r}) + \mu|\widetilde{S}(\mathbf{r})|^2 - V^{\mathrm{ext}}(\mathbf{r})C_1(\mathbf{r})\right] d^2 r. \quad (3.37)$$

In this formalism, the equilibrium condition $\delta E^{\mathrm{el}}/\delta\widetilde{u} = 0$ is

$$\widetilde{\nabla}\frac{\delta E^{\mathrm{el}}}{\delta\widetilde{C}} + \widetilde{\nabla}^*\frac{\delta E^{\mathrm{el}}}{\delta\widetilde{S}} = 0 \qquad \Longrightarrow \qquad B\widetilde{\nabla}C_1 + \mu\widetilde{\nabla}^*\widetilde{S} + \widetilde{f}^{\mathrm{ext}} = 0. \quad (3.38)$$

This equation must be considered together with the compatibility equation $\widetilde{\nabla}^*\widetilde{S} - \widetilde{\nabla}\widetilde{C} = 2i\widetilde{B}$. Thus, using the $\widetilde{C}$-picture of elasticity, we can simplify the **Classical Elasticity in a single and local fundamental equation**, given by

$$\widetilde{\nabla}(BC_1+\mu\widetilde{C})+i2\mu\widetilde{B}+\widetilde{f}^{\mathrm{ext}}=0, \tag{3.39}$$

which, using equation (), has the general solution

$$\widetilde{\overline{C}}(\mathbf{r})=-\frac{1}{2\pi}\int\left[i2\mu\widetilde{B}(\mathbf{r}')+\widetilde{f}^{\mathrm{ext}}(\mathbf{r}')\right]\frac{(\widetilde{r}-\widetilde{r}')^*}{|\mathbf{r}-\mathbf{r}'|^2}\,\mathrm{d}^2r'+\widetilde{\overline{C}}^{\,\mathrm{bc}}(\mathbf{r}), \tag{3.40}$$

where $\overline{C}_1=(B+\mu)C_1$ and $\overline{C}_2=\mu C_2$.

The local character of equation (3.39) would not be possible in the $\widetilde{S}$-picture, that is, the equation would have terms depending on the values of $\widetilde{S}$ at distant positions. On the other side, the PK force for dislocation glide in the $\widetilde{C}$-picture would have nonlocal dependence on $\widetilde{C}$, while it is local in the $\widetilde{S}$-picture. In the latter, it becomes clear that the dislocation glide is induced only by local background shear deformations. We have

$$\widetilde{f}^{\mathrm{PK}}=-i\big[B\widetilde{b}C_1^{\mathrm{bg}}(\mathbf{r}^{\mathrm{d}})+\mu\widetilde{b}^*\widetilde{S}^{\mathrm{bg}}(\mathbf{r}^{\mathrm{d}})\big] \tag{3.41}$$

and then the glide component is given by

$$f_{\mathrm{glide}}^{\mathrm{PK}}=\hat{\mathbf{b}}\cdot\mathbf{f}^{\mathrm{PK}}=\mu\ b\ S_{\mathrm{res}}^{\mathrm{bg}}(\mathbf{r}^{\mathrm{d}}), \tag{3.42}$$

where $\hat{\mathbf{b}}=\mathbf{b}/|\mathbf{b}|$ and

$$S_{\mathrm{res}}=\mathrm{Im}\left[\widetilde{S}\left(\widetilde{\hat{b}}^{\,2}\right)^*\right]=S_2\big(\hat{b}_x^2-\hat{b}_y^2\big)-S_1 2\hat{b}_x\hat{b}_y=2\left[\varepsilon_{xy}\big(\hat{b}_x^2-\hat{b}_y^2\big)-(\varepsilon_{xx}-\varepsilon_{yy})\hat{b}_x\hat{b}_y\right] \tag{3.43}$$

is called **resolved shear**. Although other types of forces can appear due to other types of deformation, as we will investigate in the next chapters, the PK force is the most predominant in usual physical systems.

In fact, background resolved shears induce dislocation glide since such movement deforms the crystal locally, shearing it contrary to the background shear, as we will see in the discussion of figure 5, in chapter 4. Consequently, the total shear $\widetilde{S}$ decreases in modulus. Moreover, the dislocation glide do not alters the density, and thus preserves C_1. Therefore, in the search for minimum energy (equation ()), **a system where dislocations can be nucleated, moved and annihilated can achieve a configuration with almost no shear and no dislocations**. In such case, the resulting configuration has only conformal deformations, since $\widetilde{S}=0$ implies that the displacement field components satisfy the Cauchy-Riemann equations. This type of configuration is called a **conformal crystal** and it has been observed in systems which are inhomogeneous and near the ground state (PIERAŃSKI, 1989; MENEZES; SILVA, 2017; SILVA et al., 2020; MENG; GRASON, 2021). One example is the one shown in figure 1.

3.2.4 The Volterra solutions for the deformation fields of a dislocation

As commented in the end of section 2.3, where we obtained the singular deformations fields $\widetilde{C}^{\text{sing}}$ and $\widetilde{S}^{\text{sing}}$, the dislocation needs an additional regular deformation for it to be in equilibrium. We can evaluated this from equation (3.39), considering the presence of a dislocation $\mathbf{B} = \mathbf{b}\ \delta(\mathbf{r})$ at the origin and no external forces. The total solutions for such problem of Classical Elasticity are called the **Volterra solutions**. By using equation (3.40) and neglecting boundary conditions contributions, the solution in our case is simply

$$\widetilde{\widetilde{C}}^{\text{V}} = -i2\mu\widetilde{b}\ \widetilde{\widetilde{\nabla}}^{*}G, \tag{3.44}$$

where $G(\mathbf{r})$ is the Green function introduced in section 2.2.3. From $\widetilde{\widetilde{C}}^{\text{V}}$ we can directly obtain $\widetilde{C}^{\text{V}}$, which has a regular part $\widetilde{C}^{\text{reg}} = \widetilde{C}^{\text{V}} - \widetilde{C}^{\text{sing}}$ given by

$$\widetilde{C}^{\text{reg}} = -\frac{i\left(B\ \widetilde{b}^{*}\widetilde{\nabla} + \mu\ \widetilde{b}\ \widetilde{\nabla}^{*}\right)G}{B+\mu}, \tag{3.45}$$

where we used the result of equation (2.51) for the singular part.

As $\widetilde{C}^{\text{reg}} = \widetilde{\nabla}^{*}\widetilde{u}^{\text{reg}}$ and $\widetilde{\nabla}\widetilde{S}^{\text{reg}} = \widetilde{\nabla}^{*}\widetilde{C}^{\text{reg}}$, we can use equations (2.47) and (2.45) to obtain, respectively,

$$\widetilde{u}^{\text{reg}} = -\frac{i\left(B\ \widetilde{b}^{*}\widetilde{\hat{r}}^{2} + 2\ \mu\ \widetilde{b}\ \ln|\mathbf{r}|\right)}{4\pi(B+\mu)}, \tag{3.46}$$

and

$$\widetilde{S}^{\text{reg}} = \frac{i\left(B\ \widetilde{b}^{*}\widetilde{\hat{r}}^{2} - \mu\ \widetilde{b}\right)\widetilde{\nabla}G}{B+\mu}. \tag{3.47}$$

Finally, in explicit form, the Volterra solutions for the total deformation fields $\widetilde{C}^{\text{V}} = \widetilde{C}^{\text{sing}} + \widetilde{C}^{\text{reg}}$ and $\widetilde{S}^{\text{V}} = \widetilde{S}^{\text{sing}} + \widetilde{S}^{\text{reg}}$ are

$$\widetilde{C}^{\text{V}} = -\frac{i\left[B\ \widetilde{b}^{*}\widetilde{\nabla} + (B{+}2\mu)\ \widetilde{b}\ \widetilde{\nabla}^{*}\right]G}{B+\mu} = -\frac{i\left[B\ \widetilde{b}^{*}\widetilde{\hat{r}} + (B{+}2\mu)\ \widetilde{b}\ \widetilde{\hat{r}}^{*}\right]}{2\pi(B+\mu)|\mathbf{r}|} \tag{3.48}$$

and

$$\widetilde{S}^{\text{V}} = \frac{iB\left[\widetilde{b} + \widetilde{b}^{*}\widetilde{\hat{r}}^{2}\right]\widetilde{\nabla}G}{B+\mu} = \frac{iB\left[\widetilde{b} + \widetilde{b}^{*}\widetilde{\hat{r}}^{2}\right]\widetilde{\hat{r}}}{2\pi(B+\mu)|\mathbf{r}|}. \tag{3.49}$$

In particular,

$$\varepsilon^{\text{V}}_{ii}(\mathbf{r}) = C^{\text{V}}_{1}(\mathbf{r}) = \frac{\mu\ \hat{\mathbf{r}}\wedge\mathbf{b}}{\pi(B+\mu)|\mathbf{r}|} \tag{3.50}$$

and

$$\varepsilon_{xy}^{\mathrm{V}}(\mathbf{r}) = \frac{1}{2} S_2^{\mathrm{V}}(\mathbf{r}) = \frac{B\ \mathrm{Re}\left[\widetilde{b}\ \widetilde{\hat{r}} + \widetilde{b}^{*}\widetilde{\hat{r}}^{3}\right]}{4\pi(B+\mu)|\mathbf{r}|}. \tag{3.51}$$

3.2.5 Dislocation dipole in a box with PBC

Consider a perfect 2D triangular crystal with Periodic Boundary Conditions (PBC) in a rectangular box $(x, y) \in \big[-L_x/2, L_x/2\big] \times \big[-L_y/2, L_y/2\big]$. A dipole of dislocations with $\mathbf{b} = \pm a_0 \hat{\mathbf{x}}$ at positions $\mathbf{r}^{\mathrm{d}} = (\pm d/2, 0)$, respectively, is then formed from the perfect crystal in the slip line $y = 0$. If $\mathbf{u}^{\mathrm{disl}}(\mathbf{r})$ is the displacement vector generated by a dislocation with $\mathbf{b} = a_0 \hat{\mathbf{x}}$ at the origin, then the displacement vectors of the dislocations in our system are given by

$$\mathbf{u}^{\mathrm{disl},\pm}(x, y) = \pm \mathbf{u}^{\mathrm{disl}}(x \mp d/2, y). \tag{3.52}$$

Note that the dipole formation (out of the perfect crystal) generates a discontinuity in u_x, which increases by a_0 when passing from the region $y < 0$ to the region $y > 0$ through the line segment between the dislocations, i.e., $-d/2 < x < d/2$. Thus, the dipole formation adds a deformation with $\partial_y u_x^{\mathrm{df}} = a_0 \delta(y)$ for $-d/2 < x < d/2$, i.e.,

$$\partial_y u_x^{\mathrm{df}}(x, y) = a_0 \delta(y) \big[H(x + d/2) - H(x - d/2)\big], \tag{3.53}$$

where $H(x)$ is the Heaviside step function, that is, 1 if $x > 0$ and 0 if $x \leq 0$.

The PBC impose that the total deformations satisfy

$$u_i^{\mathrm{tot}}(-L_x/2, y) = u_i^{\mathrm{tot}}(L_x/2, y) \quad \text{and} \quad u_i^{\mathrm{tot}}(x, -L_y/2) = u_i^{\mathrm{tot}}(x, L_y/2), \tag{3.54}$$

for any x and y, which then implies in the constraint

$$\int_{cell} \partial_j u_i^{\mathrm{tot}} \mathrm{d}^2 r = \int_{-Ly/2}^{Ly/2} \int_{-Lx/2}^{Lx/2} \partial_j u_i^{\mathrm{tot}} \mathrm{d}x \mathrm{d}y = 0, \tag{3.55}$$

for any i and j. Therefore, the dislocations of equation (3.52), which do not satisfy equations (3.54) and (3.55), induces additional deformations which can be obtained by the method of images, where the image dislocations are located at $(nL_x \pm d, mL_y)$, with $n, m \in \mathbb{Z}$. On the other hand, the deformation due to the dipole formation, expressed in equation (3.53), induces an additional deformation with a homogeneous strain $\partial_y u_x^{\mathrm{bg,df}}$ that can be obtained through

$$\int_{cell} \partial_j (u_i^{\mathrm{df}} + u_i^{\mathrm{bg,df}}) \mathrm{d}^2 r = 0 \implies (\partial_y u_x^{\mathrm{bg,df}}) L_x L_y = -\int_{cell} \partial_y u_x^{\mathrm{df}} \mathrm{d}^2 r \tag{3.56}$$

$$= -a_0 \int_{cell} \delta(y) \big[H(x + d/2) - H(x - d/2)\big] \mathrm{d}^2 r = -a_0 d$$

and then

$$\varepsilon_{xy}^{\mathrm{bg,df}} = \frac{\partial_y u_x^{\mathrm{bg,df}}}{2} = -\frac{a_0 d}{2L_x L_y} \tag{3.57}$$

This uniform background strain is a response of the system as the dislocation movement leaves a resolved shear behind, independently of what makes it move, as it is commented in the discussion of figure 5 in chapter 4.

The resolved component of the shear strain (i.e., ε_{xy}) acting on each dislocation due to the interaction with the other one and its periodic images, can be well approximated by the Volterra solution, since their distances are $\gg a_0$. For each image at a distance $\Delta\mathbf{r}$, this is given by

$$\varepsilon_{xy}^{\mathrm{V,int}}(\Delta x, \Delta y) = -\frac{\beta a_0}{2\pi} \frac{\Delta x(\Delta x^2 - \Delta y^2)}{|\Delta\mathbf{r}|^4}, \tag{3.58}$$

where $\beta = B/(B+\mu)$. Therefore, the total background resolved shear is

$$\varepsilon_{xy}^{\mathrm{bg}} = \varepsilon_{xy}^{\mathrm{bg,df}} + \sum_{n\in\mathbb{Z},m\in\mathbb{Z}} \varepsilon_{xy}^{\mathrm{V,int}}(d + nL_x, mL_y). \tag{3.59}$$

There are closed forms for infinite series that are useful in evaluating equation (3.59) and other similar sums, namely,

$$\sum_{n\in\mathbb{Z}} \frac{a^2 - (b+n)^2}{[a^2 + (b+n)^2]^2} = \pi^2 \,\mathrm{Re}\left[\mathrm{csch}^2[\pi(a+ib)]\right] \tag{3.60}$$

$$= -\pi^2 \,\mathrm{Re}\left[\csc^2[\pi(b+ia)]\right], \tag{3.61}$$

and

$$\sum_{n\in\mathbb{Z}} \frac{b}{(a+n)^2 + b^2} = -\pi \,\mathrm{Im}\left[\cot[\pi(a+ib)]\right], \tag{3.62}$$

where a and b are real.

We can use the fact that the sum in m in equation (3.59) is absolutely convergent and has a closed form, as it was shown in the previous paragraph, to obtain

$$\varepsilon_{xy}^{\mathrm{bg}} = -\frac{a_0 d}{2L_x L_y} - \frac{\pi\beta a_0}{2L_y^2} \sum_{n\in\mathbb{Z}} (d + nL_x)\mathrm{csch}^2\left[\pi\frac{(d+nL_x)}{L_y}\right], \tag{3.63}$$

where now the sum in n converges rapidly as $|n|$ increases. As it will be discussed in chapter 5, this resolved shear acts as a force of attraction between the dislocations in the PBC cell.

4 THE CORE FORCE

4.1 SOME ASSUMPTIONS ABOUT THE CORE FORCE

Our work investigates the **core force** through simulation and theory. By “core force”, we mean the phenomenon of background strain/stress gradients being responsible for a driving force on dislocations. Before going further, we make some initial assumptions about this force and discuss some of their consequences. They are intuitive guesses that will be probed in the next chapter, via simulations.

4.1.1 Effective existence of the core force

Although previous works (CLOUET, 2011; IYER; RADHAKRISHNAN; GAVINI, 2015; DAS; GAVINI, 2017) have predicted the core force, a direct observation (i.e., via simulation or experiment) is needed in order to confirm its effective action. This is because such works did not investigate how the background strain gradients can affect barriers to movement (such as the Peierls-Nabarro or a possibly new one) which could, in principle, strengthen when in the presence of them.

In fact, it is known that the PN barrier is affected by the background strain (HU et al., 2019). Thus, if this barrier is also proportional to the background strain gradients, it can cancel out or just weaken the effective intensity of the core force. In our work, we performed simulations that can probe if the observed core force is effectively a driving one, i.e., capable of driving a dislocation.

4.1.2 Driving force definition and the separation between PK and core forces

The driving force on a dislocation, $\mathbf{f}^{\mathrm{disl}}$, is defined through

$$\delta E^{\mathrm{disl}} = -\mathbf{f}^{\mathrm{disl}} \cdot \delta \mathbf{r}^{\mathrm{d}}, \tag{4.1}$$

where δE^{disl} is the variation of the total dislocation energy when this defect moves by $\delta \mathbf{r}^{\mathrm{d}}$. Classical Elasticity evaluation of equation (4.1) leads to the so called Peach-Koehler force $\mathbf{f}^{\mathrm{PK}}$ (PEACH; KOEHLER, 1950). We consider that the core force $\mathbf{f}^{\mathrm{core}}$ is not a modification of the PK force, but another type of driving force to be added, such that the total driving force on the dislocation is

$$\mathbf{f}^{\mathrm{disl}} = \mathbf{f}^{\mathrm{PK}} + \mathbf{f}^{\mathrm{core}}. \tag{4.2}$$

Moreover, while $\mathbf{f}^{\mathrm{PK}}$ depends only on the background strains $\varepsilon_{ij}^{\mathrm{bg}}$, we consider that $\mathbf{f}^{\mathrm{core}}$ depends only on the derivatives (i.e., first gradients and possibly higher order ones) of $\varepsilon_{ij}^{\mathrm{bg}}$.

4.1.3 Possible properties of the core force

Our simulations are done in the regime of small strains and small strain gradients. This allows us to probe some properties of the core force. We expect that, in this regime, it has the linearity property, i.e.,

$$\begin{aligned}\mathbf{f}^{\mathrm{core}} &= \mathbf{f}^{\mathrm{core}}(\boldsymbol{\nabla}\varepsilon_{ij}^{\mathrm{bg}}, \boldsymbol{\nabla}\partial_k\varepsilon_{ij}^{\mathrm{bg}}, ...) \\ &= M_{ij}\boldsymbol{\nabla}\varepsilon_{ij}^{\mathrm{bg}} + M_{kij}\boldsymbol{\nabla}\partial_k\varepsilon_{ij}^{\mathrm{bg}} + ... \ . \end{aligned} \tag{4.3}$$

The equation above is an intuitive guess about the core force behavior.

Within the regime of small deformations, the linearity property is a priori expected for the elasticity and plasticity phenomena. The core force would then be a linear response to the background strain gradients, i.e., linearly dependent on them. In fact, we expect that the core force is perturbatively well-behaved.

We assume that the tensor coefficients (M_{ij}, M_{kij}, ...) are constants of the crystal, depending only on the glide direction. Thus, this force obeys the uniqueness property. In other words, the uniqueness means that $\mathbf{f}^{\mathrm{core}}$ depends only on the present crystal configuration and not on its history. It does not depend on where the dislocation was before, for example.

The given core force is also symmetric under Burgers vector inversion. This is not the case for the PK force, which has an explicit dependence on the Burgers vector $\mathbf{b}$, given by (HIRTH; LOTHE, 1982; PHILLIPS, 2001)

$$\begin{aligned}\mathbf{f}^{\mathrm{PK}} &= \mathbf{f}^{\mathrm{PK}}(\varepsilon_{ij}^{\mathrm{bg}}) \\ &= \boldsymbol{\sigma}^{\mathrm{bg}} \cdot \mathbf{b} \times \hat{\mathbf{z}}, \end{aligned} \tag{4.4}$$

where $\sigma_{ij}^{\mathrm{bg}} = C_{ijkl}\varepsilon_{kl}^{\mathrm{bg}}$ is the background stress.

Finally, note that the derivatives in equation (4.3) are evaluated at the dislocation position. Thus, $\mathbf{f}^{\mathrm{core}}$ satisfies the locality property. In other words, the force depends only on the crystal configuration very near the dislocation. This is expected if such force is indeed originated from the interaction between the background and the dislocation core structure.

4.1.4 Summary of the properties to be probed by simulations

The previous assumptions are yet to be confirmed. In summary, atomistic simulations or experiments are needed in order to probe the following properties of the force:

(i) **effective driving action, i.e., the capability to move a dislocation through this force**;

(ii) **linear dependence on the background strain derivatives**;

(iii) **uniqueness**;

(iv) **symmetry under Burgers vector inversion**;

(v) **locality**.

The item (i) seems to be the most obvious one, but it still needs to be verified, as we commented in section 4.1.1.

Our simulations presented in this paper have observed dislocations gliding due to strain gradient forces, as shown in figure 5, where all the properties (i)-(v) are satisfied. In section 8.1, we show how the confirmation of each of these properties can be used to discard some theoretical proposals for the core force.

4.1.5 Consequences for dislocation interactions - size effects and nonreciprocity

The force between dislocations can be obtained from the background strains that they induce on one another. For the Classical Linear Elasticity Theory, the leading contributions to the deformation fields induced by a dislocation are exactly solvable and are called the Volterra solutions (HIRTH; LOTHE, 1982; PHILLIPS, 2001). Within such theory, the PK and core forces on a dislocation at $\mathbf{r}^{(\alpha)}$ due to another one at $\mathbf{r}^{(\beta)}$ behave as

$$\mathbf{f}^{\mathrm{PK}}_{\beta\to\alpha} \propto 1/|\mathbf{r}^{(\alpha)}-\mathbf{r}^{(\beta)}| \qquad \text{and} \qquad \mathbf{f}^{\mathrm{core}}_{\beta\to\alpha} \propto 1/|\mathbf{r}^{(\alpha)}-\mathbf{r}^{(\beta)}|^2, \tag{4.5}$$

respectively, where we considered the core force only up to first gradients. If we consider the PK force alone, the resulting power-law dynamics has no intrinsic length scale and obeys the so-called similitude principle (ZAISER; SANDFELD, 2014), leading to a dislocation dynamics that is qualitatively independent of size.

With the additional consideration of $\mathbf{f}^{\mathrm{core}}$, the total interaction loses the single power-law character and an intrinsic length scale appears, leading to a fundamental

origin of size effects. Another type of correction to the Classical PK interaction which behaves similarly to the core force (i.e., with $\propto 1/|\mathbf{r}^{(\alpha)} - \mathbf{r}^{(\beta)}|^2$), but with a different angular dependence, is the PK force due to the core-field strain and has been investigated as a possible origin of size effects (HENAGER JR; HOAGLAND, 2004; IRANI et al., 2022).

Figure 5 – Sequence of equilibrium configurations inside the same part of the system where we can see a dislocation that glided due to the action of the core force induced by $\partial_x \varepsilon^{\mathrm{bg}}_{xx}$. On the right side of the figure, the neighborhood of the particle marked by a green cross is evidenced. In (a), the dislocation, represented by the particles with 5 (red) and 7 (blue) neighbors in the Voronoi tessellation, is in equilibrium. Here, a small PK force pointing to the left is counterbalanced by a core force pointing to the right. The light blue shown in the background illustrates the variation in $\varepsilon^{\mathrm{bg}}_{xx}$, increasing in the right direction. (b) As we increase the strain gradient in the background of the dislocation position, the defect moves to the right, reaching a new position where the strain gradient is smaller and the core force equals PK again, and then it equilibrates. As we can see from the change in the region around the particle marked by a green cross, the dislocation glide induced a negative resolved shear deformation (i.e., $-\varepsilon^{\mathrm{bg}}_{xy}$).

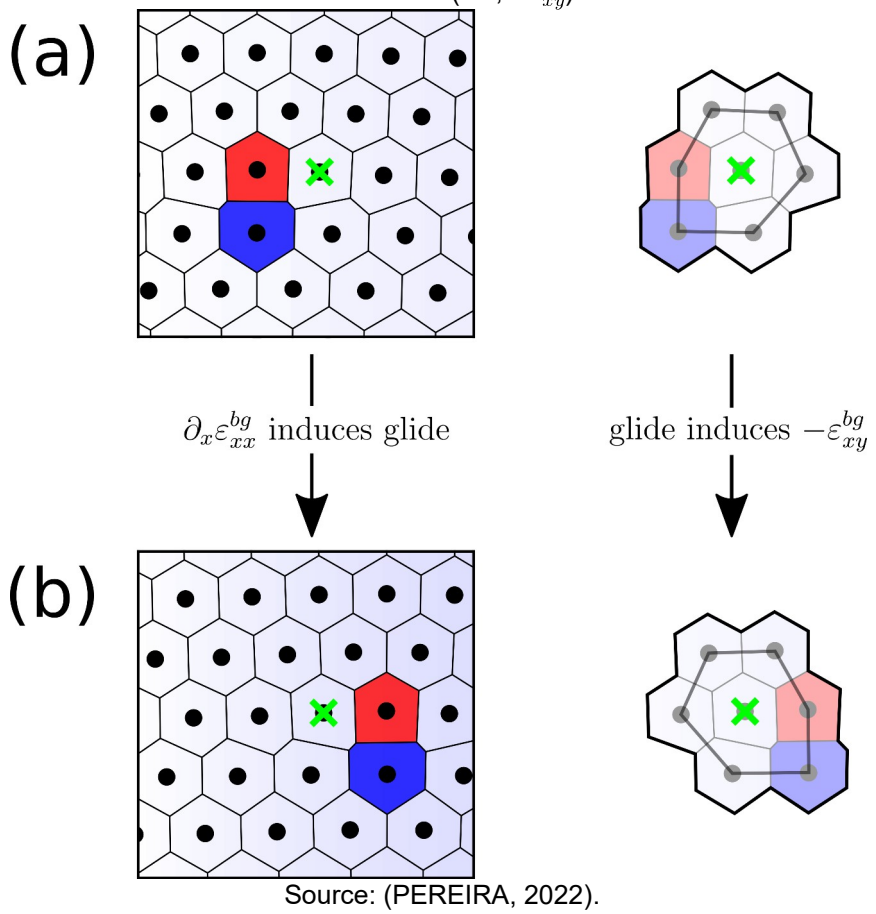

Source: (PEREIRA, 2022).

For the dislocation interactions in equation (4.5), an interesting analysis can be made for the case of a system with identical dislocations. In this case, we have

$$\mathbf{f}^{\mathrm{PK}}_{\beta\to\alpha} = -\mathbf{f}^{\mathrm{PK}}_{\alpha\to\beta} \qquad \text{and} \qquad \mathbf{f}^{\mathrm{core}}_{\beta\to\alpha} = \mathbf{f}^{\mathrm{core}}_{\alpha\to\beta}, \tag{4.6}$$

which are consequences of the Volterra strain properties $\varepsilon_{ij}^{\mathrm{V}}(\mathbf{r}) = -\varepsilon_{ij}^{\mathrm{V}}(-\mathbf{r})$ and $\boldsymbol{\nabla}\varepsilon_{ij}^{\mathrm{V}}(\mathbf{r}) = \boldsymbol{\nabla}\varepsilon_{ij}^{\mathrm{V}}(-\mathbf{r})$. This means that the core force provides nonreciprocal interactions between the dislocations. It can be shown that the PK force due to the core-field strain also has this nonreciprocity. Such type of interaction violates Newton's third law and has been extensively studied recently (VAULINA; LISINA; LISIN, 2015; LOOS; KLAPP, 2020; BRAVERMAN et al., 2021; PONCET; BARTOLO, 2022). When two “particles” interact like this, they can, e.g., drive each other indefinitely through the system, under some conditions.

4.2 HOW TO SIMULATE THE CORE FORCE

In this section, we discuss the theoretical motivations for the choice of our simulation model. The basic theoretical equations that we consider here were introduced in chapter 3. We want to test the form of the core force given in equation (4.3) as a proposed correction for the PK force of equation (3.42). Considering this, the glide component of the driving force (4.2) on a dislocation with $\mathbf{b} = b\,\hat{\mathbf{x}}$ in a triangular crystal is given by

$$f_x^{\mathrm{disl}} = 2\mu b\varepsilon_{xy}^{\mathrm{bg}} + M_{ij}\partial_x\varepsilon_{ij}^{\mathrm{bg}} + M_{kij}\partial_x\partial_k\varepsilon_{ij}^{\mathrm{bg}} + \dots\,, \tag{4.7}$$

where the background strains and their derivatives are evaluated at the dislocation position. Here, we comment some precautions that, if taken, allow us to obtain good numerical precision in our investigations. In the next chapter, we detail the simulation setup that we chose to use, comment its advantages and show the simulation results.

4.2.1 Numerical precision in the measurings of the core force properties

Quantitative investigations about the influence of the background strain derivatives on dislocation dynamics are not straightforward to do. They obviously require the precise knowledge of the background strain fields on each dislocation and of the core force acting on it.

In this section, we explain how to obtain, in simulations, precise measures of the dislocation position, the background strains on it and the resulting core force.

4.2.1.1 Dislocation position

In order to study the glide movement, we need a correct way to identify the position of a dislocation along its glide line. By showing Voronoi diagrams of crystal configurations, figure 6 illustrates how such movement occurs.

Figure 6 – Steps of an adiabatic dislocation glide in the $\hat{x}$-direction, as observed in a simulation. The Voronoi diagrams have the same coloration as in figure 5. In (a), a PK force to the left is counterbalance by a core force to the right. In the subsequent steps, we increase the core force by slightly increasing the background strain gradient at the dislocation position and wait till the configuration equilibrates. The resulting configuration of each step is shown in (b), (c) and (d). The dotted vertical line on the right is a guide to the eye in order to show the "tilting" of the dislocation at each step of the glide.

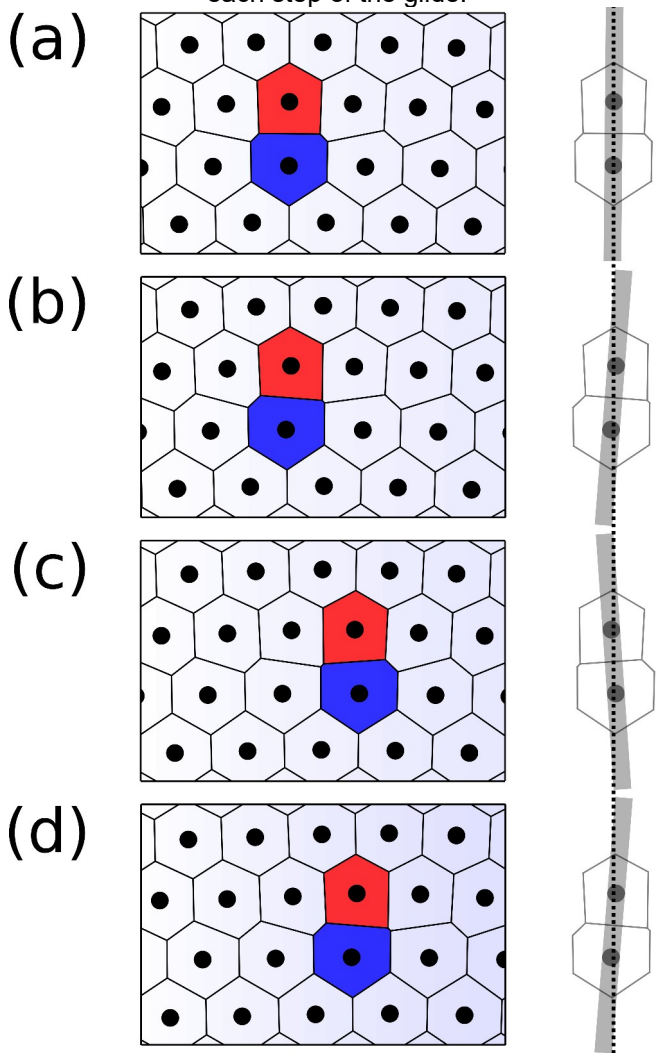

Source: (PEREIRA, 2022).

In figure 6(a), a PK force to the left is counterbalance by a core force to the right. Then, by slightly increasing the background strain gradient at the dislocation position, we increase a little the core force. As a consequence, the dislocation

“moves” to the right until it reaches a position where the forces equilibrate again. The resulting configuration is shown in (b). The “movement” turns out to be a tilting of the line connecting the disclination particles, which are the particles that represent the dislocation in a Voronoi tesselation and have 5 (red) and 7 (blue) neighbors. On the right side of figure 6, the line connecting disclination particles is compared with a vertical dotted line in order to show the tilting. By comparing (a) and (b), we can hardly say how much the dislocation “moved” in the glide direction (i.e., in the $\hat{\mathbf{x}}$-direction). The unique visible difference is that the disclination particles are vertically aligned in (a) and tilted to the right in (b). By repeating the procedure, increasing the core force and waiting equilibration, we obtain the configuration in (c). In this case, there occurred a change in the disclination particles but they continue to be tilted (this time to the left). Repeating of the procedure again now tilts the disclinations to the right, as shown in (d).

From figure 6(a) to (d), the dislocation moved. If we define the dislocation position as simply the mean position between the disclination particles, the dislocation movement would be discontinuous, having a hop from (b) to (c). But the system configuration changes continuously. There may be a way to define the dislocation position such that it changes continuously during the glide. This would be a more appropriate definition to be used when comparing simulation results with a theory (which is continuous). Without knowing such definition, only in cases as the one in (a) we can precisely locate the dislocation position along the $\hat{\mathbf{x}}$-direction, due to the vertical alignment of the disclinations.

In our simulations, we choose to consider only the situations in which the disclinations are aligned perpendicularly to the glide line. Therefore, in the glide of figure 6, we would consider the configuration (a) and a configuration that is between (c) and (d) and for which the vertical alignment happens. The disclinations' positions then provide the exact dislocation position along the glide line. When they are not aligned in this way, we have some uncertainty about the dislocation position. Our investigations need an uncertainty much smaller than the lattice constant.

4.2.1.2 Background strains

A direct observation of the crystal configuration around a dislocation provides the *total* strain fields. These are the resulting deformations generated by all the

sources of strains, such as the dislocation itself, other defects, boundary conditions, external body force fields, etc.

In order to evaluate only the background strain fields on a given dislocation (i.e., the ones generated by all the sources except by the dislocation itself), we need to use a theoretical framework that gives how each source (or group of sources) of strain acts. This can easily be done if the system is well described by the Classical Linear Hyperelasticity (or simply Classical Elasticity) theory of elastic deformations. This is the case for our simulations, which occurs in the linear regime.

4.2.1.3 Core force magnitude

In general, the PK and the core forces act simultaneously to drive the dislocation. Classical Elasticity can be used to evaluate the PK force with good approximation. Resistances to movements may also be present. By knowing the PK and the resistances and by measuring the total force, we can obtain the core force.

But without knowing the correct mobility law of dislocation dynamics in the system, we cannot measure the total force on the dislocation by measuring its movement. Unless the system is in static equilibrium, and then the total force is certainly zero. This also avoids the consideration of nonequilibrium effects in the theory. Also, if the resistances to movement are negligible, equations simplify even more and, in equilibrium, we have that the core force is simply the negative of the PK force.

Our simulations use equilibrium situations of a system with negligible resistances to movement. In these cases, we use Classical Elasticity to evaluate the PK force and then obtain the core force, which is simply the negative of $\mathbf{f}^{\mathrm{PK}}$.

5 PERFORMING SIMULATIONS OF THE CORE FORCE

5.1 SIMULATION SETUP

In our simulations, we use a model system in which we can probe all the properties of the core force (listed in section 4.1) and also measure its magnitude. It takes the precautions commented in section 4.2.1 for having better precisions in the numerical results. It also enables us good control over the system, allowing us to probe the core force properties. In the following, we describe our system and its advantages in having good knowledge and control over the strain fields and the dislocation positions.

In section 5.1.1, we tell the pair interaction between the particles and explain how its choice facilitates us to probe properties (i), (ii), (iii) and (v) of section 4.1. Then sections 5.1.2 and 5.1.3 describe the boundary conditions and the dislocations configuration, and how they facilitate the measure of the core force magnitude and the check of properties (ii), (iv) and (v). These properties are also more easy to check with the the external body force described in section 5.1.4.

5.1.1 Interparticles' interactions

The simulations have particles with power law repulsive interactions $V(r) = U_0(a_0/r)^{12}$. Interactions like this have been used as a simple model in many situations, including dislocation studies (VANSADERS; DSHEMUCHADSE; GLOTZER, 2018; KAPFER; KRAUTH, 2015). Analytical expressions for the bulk and shear moduli resulted from this interaction can be obtained by lattice sums of equation (3.7). We obtain

$$B = 21\Lambda_{12}\rho_0 U_0 \qquad \text{and} \qquad \mu = \frac{15}{2}\Lambda_{12}\rho_0 U_0, \tag{5.1}$$

where $\rho_0 = 2/(\sqrt{3}a_0^2)$ and Λ_{12} was defined in section 3.1.1.

Such type of system is useful for our analysis due to its easiness for dislocation glide (i.e., a low Peierls-Nabarro barrier, as observed in our results), facilitating the check of the effective action of a driving force such as the core force, i.e., property (i) of section 4.1. In this case, the action can happen for small strain gradients, avoiding nonlinear effects and allowing us to test the linearity (ii) property.

Moreover, the negligible Peierls-Nabarro barrier avoids the hysteresis in the movement which can appear due to the barrier. Consequently, an adiabatic “come and go” movement of the dislocation will not have hysteresis unless the force on it is not uniquely determined by the current configuration. This checks the uniqueness (iii) property.

Finally, the short-ranged character of the interaction facilitates us to probe the locality (v) property. Otherwise, in a possible occurrence of nonlocal effects, we could not track at first if their origin is in the core force or in the interparticles' interaction.

5.1.2 Periodic Boundary Conditions

Since the particles in our simulations are repulsive, they must be confined physically or by the use of Periodic Boundary Conditions (PBC). In a physical confinement, the theory could not considerate the discretization effects in the boundary precisely, since the edge has irregularities due to the crystal structure. Moreover, in PBC we can use Fourier series and the regularization commented in section 2.1.5, enabling better approximations in the formulation of Linear Elasticity.

Therefore, we use PBC in which the theory is more precise, helping us to probe the linearity (ii) and locality (v) properties commented in section 4.1. We simulate $N = 49152$ particles in a rectangular cell $(x, y) \in \left[-L_x/2, L_x/2\right]\times\left[-L_y/2, L_y/2\right]$ with $L_x = 192a_0$ and $L_y = 256(\sqrt{3}a_0/2)$, where a_0 is the lattice spacing.

5.1.3 Dislocation dipole

The PBC constrain the total Burgers vector to be zero. Therefore, other type of source for background strains must appear: other defects. We consider simulations in which we take a perfect crystal and nucleate a dipole of dislocations. They are formed in the slip line $y = 0$, have Burgers vectors $\mathbf{b} = \pm a_0\hat{\mathbf{x}}$ and positions $x = \pm d/2$, respectively, where d is the distance between them. This is what we considered in section 3.2.5.

Figure 7 illustrates the configuration of the dislocations and their images due to the PBC. The symmetric configuration in our system helps us to probe the property (iv) commented in section 4.1, i.e., the symmetry of the core force under Burgers vector inversion.

Figure 7 – Simulation box (the central one in the figure) and its images due to the PBC. In a horizontal slip line, a dipole of dislocation is formed within the perfect crystal. Then we use PK and core forces to control the dislocations' positions.

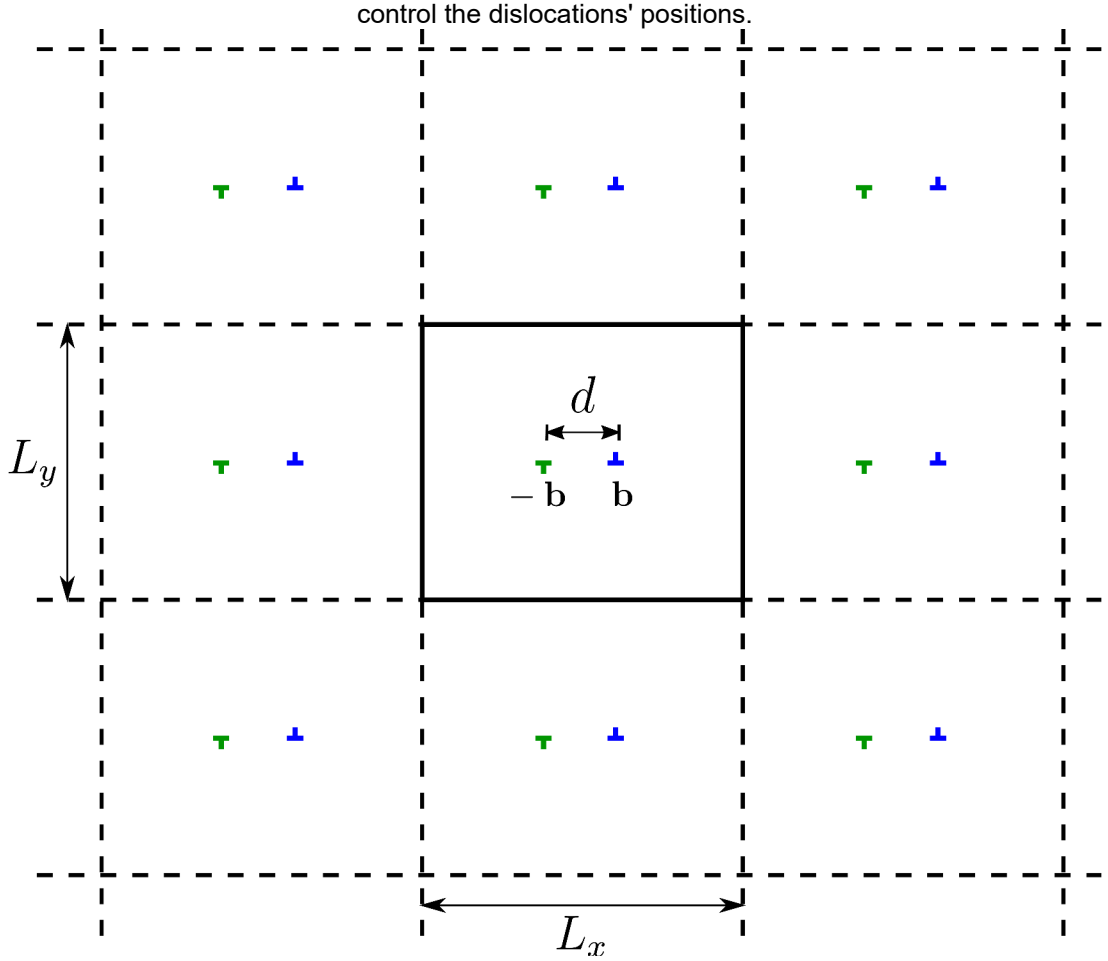

Source: (PEREIRA, 2022).

The background shear strain $\varepsilon_{xy}^{\mathrm{bg}}$ at each dislocation induced by the dipole formation and the PBC was derived in section 3.2.5 and is given by

$$\varepsilon_{xy}^{\mathrm{bg}} = -\frac{a_0 d}{2L_x L_y} - \frac{\pi\beta a_0}{2L_y^2}\sum_{n\in\mathbb{Z}}(d+nL_x)\mathrm{csch}^2\left[\pi\frac{(d+nL_x)}{L_y}\right], \tag{5.2}$$

where $\beta = B/(B+\mu)$. The first term on the r.h.s. of equation (5.2) is a result of the negative resolved shear induced by the gliding of the dislocations from the nucleation point until their current positions (separated by d), in the sense of what is shown on the right side of figure 5.

5.1.4 External body force field

Each dislocation of the dipole in PBC is subjected to a PK force of attraction to the other one. They tend to annihilate each other and return the crystal to its perfect configuration. External body force fields can be used in order to induce background

strain fields that act as configurational forces and counteract the attraction between the dislocations, keeping them apart from each other at a fixed distance d. The configurational force that we intend to induce is the core force.

We induce appropriate strain gradients in the system using 1D and radial external body forces. We use $V^{\mathrm{ext,1D}}(x) = V_0 v(x/l)$ and $V^{\mathrm{ext,rad}}(r) = V_0 v(r/l)$, where $v(x) = x^8\left(\kappa e^{-\kappa x^{10}} - e^{-x^{10}}\right)$, $\kappa = 0.35$ and $r = \sqrt{x^2 + y^2}$. We simulate for different values of the length parameter l, namely $l = 55a_0$, $57a_0$ and $59a_0$.

Figure 8 – Profile of the external potential field $V^{\mathrm{ext,1D}}(x) = V_0 v(x/l)$, where $v(x) = x^8\left(\kappa e^{-\kappa x^{10}} - e^{-x^{10}}\right)$ and $\kappa = 0.35$, and of its derivative, used in our simulations. (b) Plot of $a_0 \partial_x \varepsilon^{\mathrm{bg}}_{xx}(x)$ for the system under action of $V^{\mathrm{ext,1D}}(x)$, as derived from equation (5.3), with $l = 55a_0$, $V_0 \approx 2.94U_0$ (light red) and $V_0 \approx 5.85U_0$ (dark red). For these values of V_0, we observe the dislocations to equilibrate, respectively, at $x \approx \pm 59.5a_0$ and $x \approx \pm 62.5a_0$, as shown by A and B. The plot is shown near the position of the dislocation on the right side.

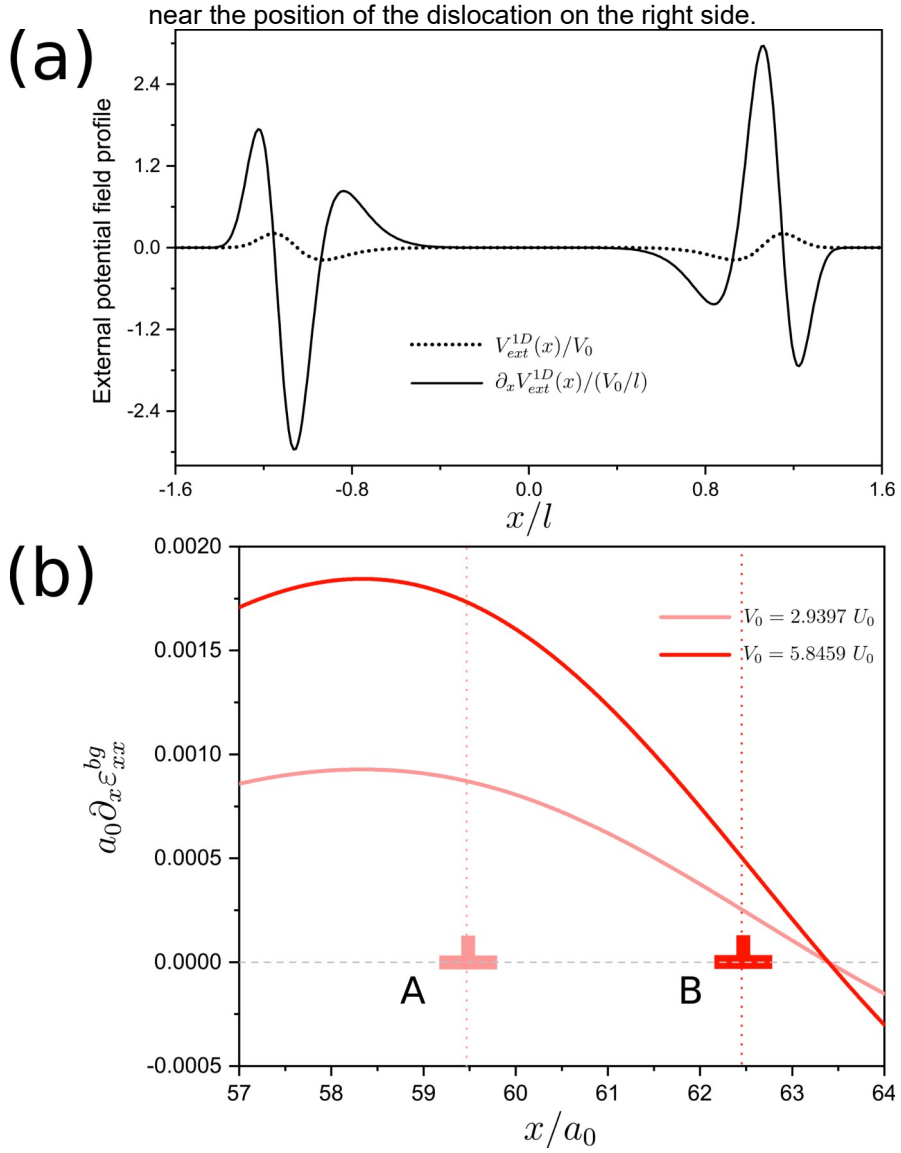

Source: (PEREIRA, 2022).

We observed that, for these choices of external potential, the dislocations can be kept apart with sufficiently small strains and strain derivatives in the system, allowing the usage of Classical Elasticity with good approximation. Such regime allows us to probe the linearity (ii) property of the core force, as commented in section 4.1. The induced background strains also have enough variation within a few lattice spacings, allowing us to probe the locality (v) property. We can use equation () to evaluate such strains. They are given by

$$\varepsilon_{xx}^{\mathrm{bg}}(x) = \frac{\rho_0 V^{\mathrm{ext,1D}}(x)}{B+\mu} \tag{5.3}$$

and $\varepsilon_{yy}^{\mathrm{bg}} = \varepsilon_{xy}^{\mathrm{bg}} = 0$ in the 1D case and by

$$\varepsilon_{yy}^{\mathrm{bg}}(x) = \frac{\rho_0}{(B+\mu)} \frac{1}{x^2} \int_0^x x' V^{\mathrm{ext,rad}}(x') \mathrm{d}x', \tag{5.4}$$

$$\varepsilon_{xx}^{\mathrm{bg}}(x) = \frac{\rho_0 V^{\mathrm{ext,rad}}(x)}{B+\mu} - \varepsilon_{yy}^{\mathrm{bg}}(x) \tag{5.5}$$

and $\varepsilon_{xy}^{\mathrm{bg}} = 0$ in the radial case.

Figure 8(a) shows the profile of $V^{\mathrm{ext,1D}}$ and its derivative. The symmetry of the external potential is convenient in order to test the core force symmetry under Burgers vector inversion (property (iv) commented in section 4.1). It is also convenient in the identification of dislocation positions, since the alignment commented in section 4.2.1.1 occurs simultaneously for both the dislocations.

5.2 SIMULATION RESULTS

As commented in section 4.2.1.3, we consider only the situations in which the dislocations are at rest. Then, by analyzing different situations like this, we can obtain how the different contributions to the force counterbalance each other. By changing the strain gradients (e.g., through a change in V_0) that are responsible for the core force contribution, the dislocations are driven to the new positions where the resulting force is zero and they equilibrate. In fact, by increasing the core force, the dislocations are driven apart, i.e., in a direction that is opposite to the PK force. This observation confirms the property (i) of section 4.1, i.e., that the core force is not a drag force but a driving one.

In our simulations, the resulting force on the dislocations is always able to drive them back and forth without any sign of hysteresis, indicating that the Peierls-

Nabarro barrier is very small. This also confirms the property (iii) of section 4.1, i.e., the uniqueness of the core force. From one equilibrium configuration to the other we use overdamped evolution for the particles in the simulations. No unstable equilibrium appears, as we probed by using a small temperature through Brownian Dynamics (SATOH, 2011).

For the system in which we apply $V^{\mathrm{ext,1D}}(x)$ with $l = 55a_0$, figure 8(b) shows the graph of the strain gradient $a_0\partial_x\varepsilon^{\mathrm{bg}}_{xx}$, as generated by the external force and evaluated through equation (5.3), near the position at which the dislocation $\mathbf{b} = +a_0\hat{\mathbf{x}}$ is equilibrated in our simulations with $V_0 \approx 2.94U_0$ (light red) and $V_0 \approx 5.85U_0$ (dark red). In this region, $\varepsilon^{\mathrm{bg}}_{xy} < 0$ and then, if we turn off the external force (i.e., set $V_0 = 0$), the dislocation shown in the figure would move to the left until it finally annihilates the other dislocation, which would be precisely at $x = 0$. We can see in the figure that, by increasing V_0, the strain gradient increases and the dislocation moves to the right until it equilibrates in a new position. The same happens simultaneously with the other dislocation in the other direction. This mirror symmetry, observed in all simulations, confirms the property (iv) of section 4.1, i.e., the Burgers vector inversion symmetry of the core force.

We gather the data of equilibrium situations (i.e., dislocations at rest with $f^{\mathrm{disl}}_x = 0$) in varying intensities of $V^{\mathrm{ext,1D}}(x)$ for the three different values of the parameter l considered. As we consider only the cases in which the dislocation positions are well-defined, as commented in section 4.2.1.1, their distances can be precisely evaluated. For these cases, we use equations (5.2) and (5.3) to evaluate the background deformations and plot in figure 9(a) the values of $-2\varepsilon^{\mathrm{bg}}_{xy}$ versus $a_0\partial_x\varepsilon^{\mathrm{bg}}_{xx}$ acting at the dislocations' equilibrated positions. Note that a linear relation is predicted for this graph if we consider equation (4.7) up to first gradient. A simple fit results in $M_{xx} \approx 1.64\mu a_0^2$, but we clearly see that the force counteracting the PK one does not depend solely on the value of $\partial_x\varepsilon^{\mathrm{bg}}_{xx}$.

In principle, the problem here could have a nonlocal origin, as we can see from figure 8(b) that the strain derivative varies greatly within a few lattice spacings. But we find that, by considering higher order derivative terms in equation (4.7) evaluated precisely at the dislocation positions, we can match the data with a good fit and then the locality property (v) of section 4.1 is valid. The motivation to consider the higher order derivative terms is discussed in the following.

Figure 9 – Relations between the background resolved shear and strain gradients on the dislocation $\mathbf{b} = +a_0\hat{\mathbf{x}}$ for equilibrium configurations in our simulations with the 1D external force field. All the deformations can be obtained from the distance between the dislocations using equations () and (). In (a) we can see that $\partial_x \varepsilon_{xx}^{\mathrm{bg}}$ alone cannot explain the force which is counterbalancing the PK one. By including a force due to $\partial_x^3 \varepsilon_{xx}^{\mathrm{bg}}$, a good fit to the data is obtained, as it is shown in (b).

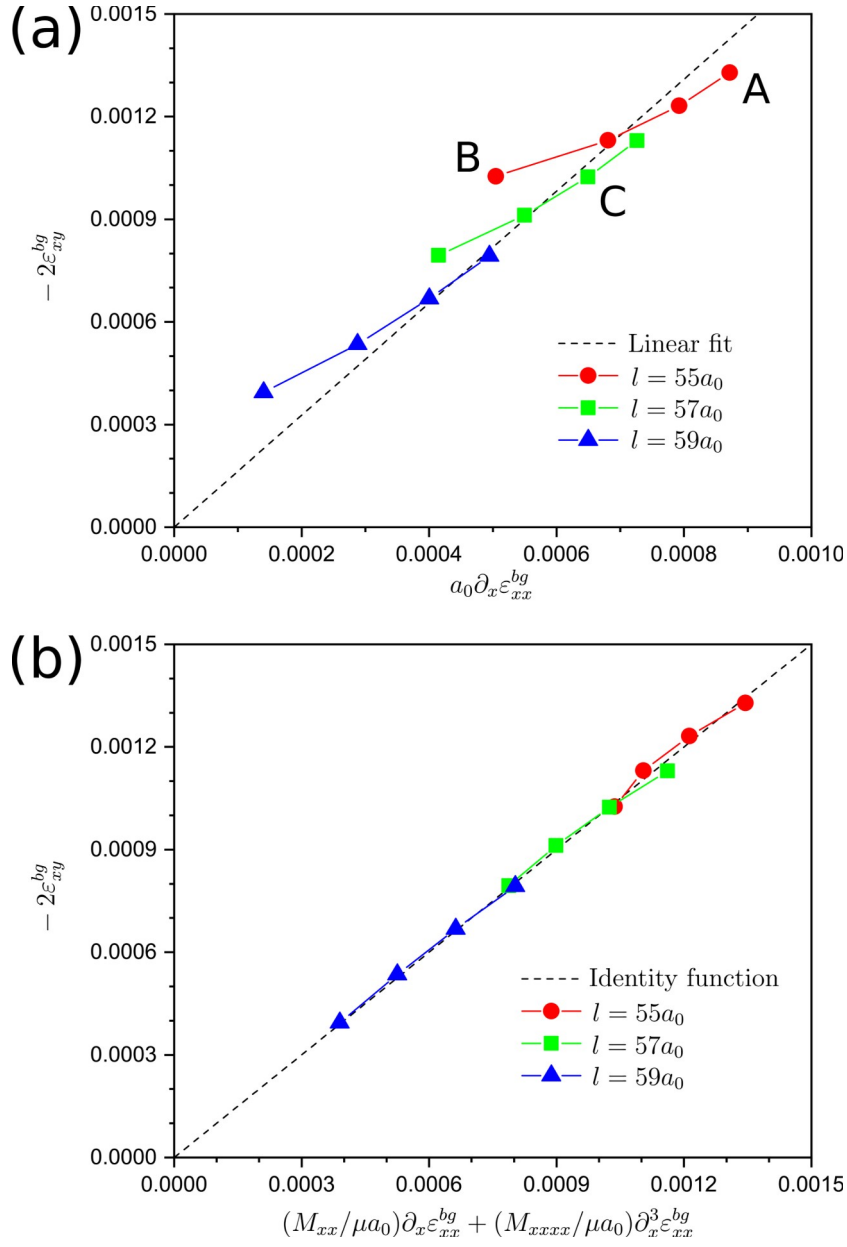

Source: (PEREIRA, 2022).

The cases A and B of figure 9(a) are the same of figure 8(b). In the transition from A to B, the dislocations are driven apart and their new equilibrium positions have smaller $|\partial_x \varepsilon_{xx}^{\mathrm{bg}}|$. If we compare the cases B and C, where C was simulated with a different external force field, we can see that the PK forces (originated from $\varepsilon_{xy}^{\mathrm{bg}}$) in them are almost equal, whereas the strain gradients $\partial_x \varepsilon_{xx}^{\mathrm{bg}}$ are different. Thus the

core force that counterbalance PK must depend on other factors that are different in these cases, such as the higher order derivatives $\partial_x^2 \varepsilon_{xx}^{\mathrm{bg}}$ and $\partial_x^3 \varepsilon_{xx}^{\mathrm{bg}}$. Locally, these derivatives are the main differences between the situations B and C of figure 9(a) besides the difference in $\partial_x \varepsilon_{xx}^{\mathrm{bg}}$. We can better fit the data by considering, for instance, an additional contribution like $M_{xxx}\partial_x^2 \varepsilon_{xx}^{\mathrm{bg}}$ (provided that M_{xxx} changes sign under a change in the sign of b) or $M_{xxxx}\partial_x^3 \varepsilon_{xx}^{\mathrm{bg}}$ in the force of equation (4.7).

In the end of section 6.1.1, we show some theoretical arguments that make us believe that the core force cannot be linear with $\partial_x^2 \varepsilon_{xx}^{\mathrm{bg}}$ and thus M_{xxx} must be zero. Using only the M_{xx} and M_{xxxx} terms in equation (4.7), the fitting of the data provides $M_{xx} \approx 2.259 \mu a_0^2$ and $M_{xxxx} \approx 7.023 \mu a_0^4$. Figure 9(b) shows how the formula for the force is greatly improved by the third gradient term. Note that all the terms used here are linear in the strains, confirming the property (ii) of section 4.1, i.e., the linearity of the core force.

Finally, we use the data for the simulations with radial forces (in which there appears $\varepsilon_{yy}^{\mathrm{bg}}$) and fit the general equilibrium condition

$$f_x^{\mathrm{disl}} \approx 2\mu b \varepsilon_{xy}^{\mathrm{bg}} + M_{xx}\partial_x \varepsilon_{xx}^{\mathrm{bg}} + M_{yy}\partial_x \varepsilon_{yy}^{\mathrm{bg}} + M_{xxxx}\partial_x^3 \varepsilon_{xx}^{\mathrm{bg}} + M_{xxyy}\partial_x^3 \varepsilon_{yy}^{\mathrm{bg}} = 0 \qquad (5.6)$$

to obtain the values $M_{yy} \approx 0.5024 \mu a_0^2$ and $M_{xxyy} \approx -17.57 \mu a_0^4$. The other background strain derivatives were not considered since their values are relatively much smaller in our system.

6 CORE ENERGY AND OTHER THEORETICAL APPROACHES

In this chapter and in the next one, we investigate some theoretical predictions about the core force that are found in the literature and also other possibilities. Unfortunately, all of them have issues and none of them were found to predict the coefficients of the core force without a direct measurement from the simulations. But many properties are correctly predicted by some approaches and interesting results are found.

We can separate the theoretical approaches into two types: continuum theory modifications and core energy analysis. Any type of continuum theory of elasticity is an approximation and its prediction about the dislocation energy must be complemented by a core energy correction. In section 6.1, we focus on the core energy consideration and try to find ways of measuring it in order to predict the core force. Also, we show a case in which we can go the other way around, i.e., use the coefficients in the core force to evaluate the core energy. In section 6.2, we show some efforts to modify the Classical Elasticity theory in order to better describe the dislocation dynamics, without resorting to core energy considerations.

6.1 CORE ENERGY AS THE ORIGIN OF THE CORE FORCE

This section investigates the core energy and its relation with the core force. Note that all the properties of the core force guessed in chapter 4 (i.e., effective driving action, linearity, uniqueness, etc.) and confirmed in chapter 6 are obeyed if we write the force of equation (4.3) in the form

$$\mathbf{f}^{\mathrm{core}} = -\boldsymbol{\nabla} E^{\mathrm{co}}\big|_{\mathbf{r}=\mathbf{r}^{\mathrm{d}}} = -\frac{\partial E^{\mathrm{co}}}{\partial \varepsilon_{ij}^{\mathrm{bg}}} \boldsymbol{\nabla} \varepsilon_{ij}^{\mathrm{bg}}\big|_{\mathbf{r}=\mathbf{r}^{\mathrm{d}}} - \frac{\partial E^{\mathrm{co}}}{\partial (\partial_k \varepsilon_{ij}^{\mathrm{bg}})} \boldsymbol{\nabla} \partial_k \varepsilon_{ij}^{\mathrm{bg}}\big|_{\mathbf{r}=\mathbf{r}^{\mathrm{d}}} - \dots , \tag{6.1}$$

where we only need to know how to evaluate the crystal's core energy function $E^{\mathrm{co}} = E^{\mathrm{co}}(\varepsilon_{ij}^{\mathrm{bg}}, \partial_k \varepsilon_{ij}^{\mathrm{bg}}, ...)$ in a unique way.

In section 6.1.1, a general definition of the core energy is given. The final evaluation of it depends on how the continuum theory is considered. Section 6.1.2 shows the standard way to do so and its problems with ambiguity are commented. Finally, in section 6.1.3, we show that, in systems with power law interactions, we can obtain the core energy from measurements of the core force.

6.1.1 General definition of the core energy

The general idea for the core energy (E^{co}) is that it represents the energetic correction necessary for the continuum theory result (E^{cont}) to match the total dislocation energy (E^{disl}) in the real crystal, i.e., $E^{\mathrm{disl}} = E^{\mathrm{cont}} + E^{\mathrm{co}}$.

The evaluation of E^{cont} depends on the theory considered and the standard one is presented in section 6.1.2. The crystal's E^{disl}, on the other hand, has a definite way to be evaluated. It is obtained from the total energy of the crystal when deformed only by the dislocation presence minus the energy of the crystal without it. By considering the crystal's energy as a function of the particles' positions, we can write

$$E^{\mathrm{disl}} = E(\{\mathbf{r}^{(\alpha)}\}) - E(\{\mathbf{r}_0^{(\alpha)}\}), \tag{6.2}$$

where $\{\mathbf{r}^{(\alpha)}\}$ and $\{\mathbf{r}_0^{(\alpha)}\}$ are the particles' positions with and without the dislocation presence, respectively. We are not using $\{\mathbf{R}^{(\alpha)}\}$ instead of $\{\mathbf{r}_0^{(\alpha)}\}$ in order to consider the possibility of having deformations at the background of the dislocation.

In practice, E^{disl} increases with the size of the crystal, diverging for infinite crystals. The continuum theory prediction also diverges. On the other hand, the core energy remains finite. Therefore, we consider energetic evaluations inside a circular region, with radius R and centered at the dislocation, and define

$$E^{\mathrm{co}} = \lim_{R\to\infty} \left[E^{\mathrm{disl}}(R) - E^{\mathrm{cont}}(R)\right]. \tag{6.3}$$

The convergence of this limit is usually fast enough, as the continuum theory becomes accurate far from the core.

Figure 10 – Illustration of the effects of $\varepsilon_{xy}^{\mathrm{bg}}$ and $\partial_x \varepsilon_{xx}^{\mathrm{bg}}$ around an edge dislocation. The reflection symmetry in the x direction implies that the change in the core energy must be the same for positive and negative values of these deformations. Therefore, this energy cannot depend linearly on them.

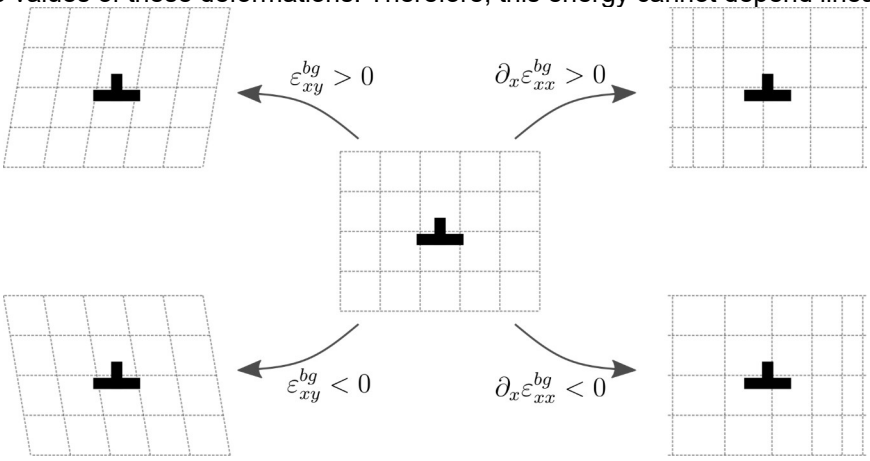

Source: (PEREIRA, 2022).

The presence of background strains can affect the core energy and some symmetric considerations can be made a priori. For instance, linear dependences of E^{co} on $\varepsilon_{xy}^{\mathrm{bg}}$ and $\partial_x \varepsilon_{xx}^{\mathrm{bg}}$ are forbidden for an edge dislocation with $\mathbf{b} = b\hat{\mathbf{x}}$, as we can see from figure 10. Consequently, the force obtained from equation (6.1) does not have terms linearly proportional to $\partial_x \varepsilon_{xy}^{\mathrm{bg}}$ or to $\partial_x^2 \varepsilon_{xx}^{\mathrm{bg}}$.

6.1.2 Ambiguity in the standard core energy

The standard way to evaluate the continuum theory prediction E^{cont} for the dislocation energy is through equation (3.22), by using the dislocation strains in the integral. The classical strain fields of a dislocation are obtained from the Volterra solution. In polar coordinates, there exist functions $h_{ij}^{\mathrm{V}}(\theta)$ such that the solution for a dislocation $\mathbf{b} = b\ \hat{\mathbf{x}}$ at the origin, have the form (HIRTH; LOTHE, 1982)

$$\varepsilon_{ij}^{\mathrm{V}}(\mathbf{r}) = h_{ij}^{\mathrm{V}}(\theta)\ \frac{b}{r}. \tag{6.4}$$

Note that the integral of equation (3.22) using Volterra strains diverges logarithmically for both large and small radii. The usual procedure to obtain E^{cont} is to integrate equation (3.22) in a region between a fixed core radius r^{co} and a larger radius $R \gg r^{\mathrm{co}}$. By doing so, the core energy is standardly defined as (HIRTH; LOTHE, 1982)

$$E^{\mathrm{co,std}} = \lim_{R\to\infty} \left[E^{\mathrm{disl}}(R) - \frac{b^2 K}{8\pi} \ln\left(\frac{R}{r^{\mathrm{co}}}\right) \right], \tag{6.5}$$

where the pre-logarithmic factor K depends on the elastic constants, e.g., $K = 4B\mu/(B+\mu)$ for the triangular crystal.

The choice of the core radius r^{co} is arbitrary and usually taken to be of the order of the Burgers vector modulus b, which is frequently the lattice spacing. By taking simulations for large values of R and using the correct K, equation (6.5) converges and $E^{\mathrm{co,std}}$ is then independent of R. See (IYER; RADHAKRISHNAN; GAVINI, 2015; PIZZAGALLI; DEMENET; RABIER, 2009; HU et al., 2019) for some recent calculations of $E^{\mathrm{co,std}}$ from simulations of straight dislocations in some relevant 3D crystals.

In order to obtain the core force through equation (6.1), we need to know how the core energy depends on the background strains. By using background deformations in the defected crystal of the simulation and measuring the

corresponding core energies, the dependence $E^{\mathrm{co,std}} = E^{\mathrm{co,std}}(\varepsilon_{ij}^{\mathrm{bg}})$ can be evaluated, as it was done in previous works (IYER; RADHAKRISHNAN; GAVINI, 2015; DAS; GAVINI, 2017). These works used the evaluated derivatives of $E^{\mathrm{co,std}}(\varepsilon_{ij}^{\mathrm{bg}})$ to predict the core force, through equation (6.1). But this core energy definition has problems with uniqueness, i.e., with the property (ii) of section 4.1, as we discuss in the following.

The standard core energy greatly depends on the choice of the core radius. Once measured for some r^{co}, the energy $\overline{E}^{\mathrm{co,std}}$ for any other core radius is $\overline{E}^{\mathrm{co,std}} = E^{\mathrm{co,std}} + (b^2 K/8\pi)\ln\left(\overline{r}^{\mathrm{co}}/r^{\mathrm{co}}\right)$. Since the factor b^2K is also a function of the background strains, in general, we have that $\partial\overline{E}^{\mathrm{co,std}}/\partial\varepsilon_{ij}^{\mathrm{bg}} \neq \partial E^{\mathrm{co,std}}/\partial\varepsilon_{ij}^{\mathrm{bg}}$. This means that the arbitrary choice of r^{co} affects the dependence $E^{\mathrm{co,std}} = E^{\mathrm{co,std}}(\varepsilon_{ij}^{\mathrm{bg}})$ and the core force of equation (6.1). As uniqueness is a confirmed property of the core force, the standard core energy is not appropriate, due to its ambiguous definition, to be used in equation (6.1).

There are some known definitions for the core-energy which are unambiguous, e.g., in the framework of the KTHNY-theory (STRANDBURG, 1988) and in the Kanzaki force approach (GURRUTXAGA-LERMA; VERSCHUEREN, 2019). The correct one to be used in equation (6.1) and then predict the correct core force acting on a dislocation is still to be discovered.

6.1.3 Crystals with power-law interactions: obtaining the core energy from the core force

By considering that equation (6.1) is valid, the measured coefficients of the core force give us the derivatives of $E^{\mathrm{co,std}} = E^{\mathrm{co,std}}(\varepsilon_{ij}^{\mathrm{bg}}, \partial_k\varepsilon_{ij}^{\mathrm{bg}}, ...)$. Here we show that there are systems in which we can obtain the absolute value of the core energy directly from its derivatives. In such cases, the core energy can be obtained from measures of the core force. This happens in systems with power-law interactions, which are known to have special relations, such as the Virial Theorem, between energy and force.

If the particles interact via a power-law potential $V_p(r) \propto 1/r^m$, we have the scaling law $E(\{\lambda\mathbf{r}^\alpha\}) = \lambda^{-m}E(\{\mathbf{r}^\alpha\})$ for the total potential energy. This is satisfied by E^{disl}, as we can see from equation (6.2), by E^{cont}, which comes from a continuum

theory, and therefore by $E^{\rm co} = E^{\rm disl} - E^{\rm cont}$. The scaling law describes how these energies depend on the density, which scales as λ^{-2}. Thus, the energies have no other dependence on the density but the power law $E \propto \lambda^{-m} \propto \rho^{m/2}$. In 2D Linear Elasticity, the density is $\propto (1 - \varepsilon_{xx}^{\rm bg} - \varepsilon_{yy}^{\rm bg})$ and then the scaling law tells us that the dependence of $E^{\rm co}(\varepsilon_{ij}^{\rm bg})$ on $(\varepsilon_{xx}^{\rm bg} + \varepsilon_{yy}^{\rm bg})$ is in the form $\propto (1 - \varepsilon_{xx}^{\rm bg} - \varepsilon_{yy}^{\rm bg})^{m/2}$, while the dependences on $(\varepsilon_{xx}^{\rm bg} - \varepsilon_{yy}^{\rm bg})$ and on $\varepsilon_{xy}^{\rm bg}$ are not known, in principle. We can write this as

$$E^{\rm co}(\varepsilon_{ij}^{\rm bg}) = \left[1 - \varepsilon_{xx}^{\rm bg} - \varepsilon_{yy}^{\rm bg}\right]^{m/2} G^{\rm co}(\varepsilon_{xx}^{\rm bg} - \varepsilon_{yy}^{\rm bg}, \varepsilon_{xy}^{\rm bg}), \tag{6.6}$$

where $G^{\rm co}$ is a function of the deviatoric deformations $\varepsilon_{xy}^{\rm bg}$ and $(\varepsilon_{xx}^{\rm bg} - \varepsilon_{yy}^{\rm bg})$ which change the shape but not the size of the crystal. If the core energy depends also on derivatives of $\varepsilon_{ij}^{\rm bg}$, i.e., if $E^{\rm co} = E^{\rm co}(\varepsilon_{ij}^{\rm bg},\ \partial_k \varepsilon_{ij}^{\rm bg},\ ...)$, we have $G^{\rm co} = G^{\rm co}(\varepsilon_{xx}^{\rm bg} - \varepsilon_{yy}^{\rm bg},\ \varepsilon_{xy}^{\rm bg},\ \partial_k \varepsilon_{ij}^{\rm bg},\ ...)$.

By taking derivatives of equation (6.6) with respect to $\varepsilon_{xx}^{\rm bg}$ and $\varepsilon_{yy}^{\rm bg}$, it is easy to show that

$$-\frac{1}{m}\left[\frac{\partial E^{\rm co}}{\partial \varepsilon_{xx}^{\rm bg}}\Big|_{\varepsilon_{ij}^{\rm bg}=0} + \frac{\partial E^{\rm co}}{\partial \varepsilon_{yy}^{\rm bg}}\Big|_{\varepsilon_{ij}^{\rm bg}=0}\right] = G^{\rm co}(0,0) = E^{\rm co}(0). \tag{6.7}$$

Therefore, by relating the derivatives of $E^{\rm co}$ in equation (6.1) with the coefficients in equation (4.3), the scaling law of equation (6.7) tells us that the core energy at zero background deformations is

$$E^{\rm co} = \frac{1}{m}\left(M_{xx} + M_{yy}\right) \tag{6.8}$$

for systems with power-law interparticle interactions $\propto 1/r^m$. With the results for M_{xx} and M_{yy} obtained from simulations in section 5.2, we find $E^{\rm co} \approx 0.23\mu a_0^2 \approx 12U_0$ for the system with $V_p(r) = U_0(a_0/r)^{12}$ and density $\rho = 2/(\sqrt{3}a_0^2)$. A definite value for the core energy can be used, e.g., to obtain the appropriate core radius through equation (6.5) and predict the melting temperature in 2D, through the KTHNY-theory (STRANDBURG, 1988).

6.2 ENERGY FUNCTIONAL MODIFICATIONS

The dislocation energy within the continuum Elasticity theory depends on the energy functional and on how the dislocation is described. In order to obtain the core force within continuum theory, here we investigate possible modifications of the

functional. In the next chapter, we investigate a modification of the dislocation description.

We recall that the Peach-Koehler force results from the Classical Elasticity functional, expressed in equation (3.22), and the Burgers vector definition, $\mathbf{b} = \oint \mathrm{d}\mathbf{u}$. In the Supplementary Material (SM) of (PEREIRA, 2022), it is derived in a similar way to what is done in section 3.2.1 but considering an additional term like $-C^{(1)}_{ijklm}\varepsilon_{ij}\partial_m\varepsilon_{kl}/2$, where $C^{(1)}_{ijklm}$ are constants, inside the integral of equation (3.22). This modification in the energy functional can provide strain gradient forces without using a core energy. It is a type of Strain Gradient Theory (SGT), that is, a continuum theory that considers relevant influences of strain gradients in the elasticity/plasticity. The correction to the PK force derived this way in the SM of (PEREIRA, 2022) is

$$f_n^{\mathrm{SGT}} = \epsilon_{nk} b_l C^{(1)}_{ijklm} \partial_m \varepsilon^{\mathrm{bg}}_{ij}. \tag{6.9}$$

It obeys properties such as uniqueness, locality and linearity but it has problems with the symmetry under the inversion $\mathbf{b} \to -\mathbf{b}$ (property (iv) of section 4.1), which was confirmed by our simulations to be valid in the observed core force.

SGTs of Elasticity which correctly obey the symmetries have long been studied (LAZAR; KIRCHNER, 2007; PO et al., 2018). For example, we can add a term $\propto \partial_k \varepsilon_{ij} \partial_n \varepsilon_{lm}$ in equation (3.22), which correctly obeys the symmetries, and obtain $\mathbf{f}^{\mathrm{disl}}$ through a procedure similar to the one used in section 3.2.1. The resulting force has a term proportional to second gradients of strains. This second gradient force is similar to the third term in the r.h.s of equation (4.7) and is originated from a generalized Elasticity Theory, without considering the core energy. Unfortunately, no correct account for a first gradient force on dislocations, with the properties that we observe in this work, was ever obtained in this way.

Another possible correction within continuum theory is to consider nonlinear terms in the energy functional. But the formal derivations of the configurational force in Nonlinear Elasticity (STEINMANN, 2002) provide only nonlinear corrections to PK, which disobey the property (ii) of section 4.1, and have no strain gradient dependence.

7 ANOTHER APPROACH WITHIN CONTINUUM THEORY: THE CORE FIELD

A formal way to describe corrections to the Volterra dislocation field is by making use of (fictious) localized forces which can generate the core field (CLOUET, 2011). This field acts as a correction to the Volterra field near the dislocation core. It represents the other terms in a Laurent series solution for the elastic fields outside the core.

In this chapter, we show how the core field approach can predict a core force which respect the properties observed in our simulations. However, it cannot quantitatively predict the coefficients of the core force, as we probed through simulations which measure the core field.

7.1 A MODIFICATION IN THE DISLOCATION DESCRIPTION - THE CORE FIELD

We can try to correct the Classical Elasticity by modifying the way we characterize a dislocation. To do so, we present here an approach that provides a prediction of the core force, as derived in (CLOUET, 2011). But, as commented further in the end of this section, we observe that it cannot predict the correct coefficients of the core force, and therefore it is quantitatively wrong.

The classical (Volterra) displacement field $\mathbf{u}^{\mathrm{V}}$ of a dislocation at the origin is the solution of the equations

$$\epsilon_{jk}\partial_j\partial_k u_i^{\mathrm{V}} = b_i\delta(\mathbf{r}) \qquad \text{and} \qquad C_{ijkl}\partial_j\partial_l u_k^{\mathrm{V}} = 0. \tag{7.1}$$

The first equation comes from the Burgers vector definition and the second one is the Classical Elasticity field equation (3.18) for zero body forces. In polar coordinates, the Volterra field has the form

$$\mathbf{u}^{\mathrm{V}}(r,\theta) = \mathbf{v}(\theta)\ln r + \mathbf{u}_0(\theta). \tag{7.2}$$

A simple way to modify such dislocation description is to consider that there are some forces acting near the dislocation core. Thus, the so-called core field $\mathbf{u}^{\mathrm{cf}}$, which is the solution of

$$C_{ijkl}\partial_j\partial_l u_k^{\mathrm{cf}} = -f_i^{\mathrm{cf}}, \tag{7.3}$$

must be considered in order to correct the Volterra approximation. Here, $\mathbf{f}^{\mathrm{cf}} = \mathbf{f}^{\mathrm{cf}}(\mathbf{r}-\mathbf{r}^{\mathrm{d}})$ is an ad hoc body force density field associated with the dislocation.

In the literature (CLOUET, 2011; HENAGER JR; HOAGLAND, 2004), $\mathbf{f}^{\mathrm{cf}}$ is usually considered as a set of point forces.

Note that the net contribution of $\mathbf{f}^{\mathrm{cf}}$ must be zero, i.e., $\int \mathbf{f}^{\mathrm{cf}}(\mathbf{r})\mathrm{d}^2r = 0$, since no net force appears in the dislocation region. Moreover, as it represents a core effect, this force must be zero outside some core radius, where Classical Elasticity is valid. Therefore, the core field decays and has the following multipole expansion

$$\mathbf{u}^{\mathrm{cf}}(r,\theta) = \mathbf{u}_1(\theta)\frac{1}{r} + \mathbf{u}_2(\theta)\frac{1}{r^2} + \mathcal{O}\left(\frac{1}{r^3}\right), \tag{7.4}$$

where $\mathbf{u}_1$ and $\mathbf{u}_2$ depend on the dipolar and quadrupolar moments of $\mathbf{f}^{\mathrm{cf}}(\mathbf{r})$, respectively.

Other constraints on $\mathbf{f}^{\mathrm{cf}}$ are necessary in order to obey the reflection symmetry of the edge dislocation. For the case $\mathbf{b} = b\hat{\mathbf{x}}$, we must have $\mathbf{f}^{\mathrm{cf}}(\mathbf{r}) = \boldsymbol{P}\cdot\mathbf{f}^{\mathrm{cf}}(\boldsymbol{P}\cdot\mathbf{r})$ for the reflection (parity) operation $\boldsymbol{P}=\left[\begin{smallmatrix}-1 & 0\\ 0 & 1\end{smallmatrix}\right]$, i.e., $f_x^{\mathrm{cf}}(x,y) = -f_x^{\mathrm{cf}}(-x,y)$ and $f_y^{\mathrm{cf}}(x,y) = f_y^{\mathrm{cf}}(-x,y)$. In this case, the contribution to the energy due to $\mathbf{f}^{\mathrm{cf}}$ interacting with the background deformation can be directly obtained from the energy functional of equation (3.21). We can make a multipole expansion and use the symmetries to simplify it, obtaining

$$\begin{aligned} E^{\mathrm{cf-bg}} &= -\int f_i^{\mathrm{cf}}(\mathbf{r})u_i^{\mathrm{bg}}(\mathbf{r})\mathrm{d}^2r \\ &\approx -\big[M_1\partial_x u_x^{\mathrm{bg}} + M_2\partial_y u_y^{\mathrm{bg}} + M_{12}\partial_x\partial_y u_x^{\mathrm{bg}} + M_{11}\partial_x^2 u_y^{\mathrm{bg}} + M_{22}\partial_y^2 u_y^{\mathrm{bg}} \\ &\quad + M_{111}\partial_x^3 u_x^{\mathrm{bg}} + M_{112}\partial_x^2\partial_y u_y^{\mathrm{bg}} + M_{122}\partial_x\partial_y^2 u_x^{\mathrm{bg}} + M_{222}\partial_y^3 u_y^{\mathrm{bg}} + \mathcal{O}(\partial^4 u^{\mathrm{bg}})\big], \end{aligned} \tag{7.5}$$

where $M_1 = \int x f_x^{\mathrm{cf}}\mathrm{d}^2r$, $M_2 = \int y f_y^{\mathrm{cf}}\mathrm{d}^2r$, $M_{12} = \int xy f_x^{\mathrm{cf}}\mathrm{d}^2r$, $M_{11} = \int (x^2/2) f_y^{\mathrm{cf}}\mathrm{d}^2r$, $M_{22} = \int (y^2/2) f_y^{\mathrm{cf}}\mathrm{d}^2r$, $M_{111} = \int (x^3/6) f_x^{\mathrm{cf}}\mathrm{d}^2r$, $M_{112} = \int (x^2y/2) f_y^{\mathrm{cf}}\mathrm{d}^2r$, $M_{122} = \int (xy^2/2) f_x^{\mathrm{cf}}\mathrm{d}^2r$ and $M_{222} = \int (y^3/6) f_y^{\mathrm{cf}}\mathrm{d}^2r$. Also, by symmetry, a change in the sign of b changes the sign of the quadrupolar moments M_{12}, M_{11} and M_{22} in equation (7.5).

Note that equation (7.5) does not represent the core energy, since it is zero when there are no background deformation, but it carries all the symmetries expected for E^{co}. The derivatives in equation (7.5) are evaluated at the dislocation position and then the energy varies as the defect moves. From equation (4.1), such variation of $E^{\mathrm{cf-bg}}$ implies in a force acting on the dislocation which has the same form of equation (4.3) and satisfies all the properties guessed in chapter 4 and confirmed in chapter 5. Up to first gradients of strains, this approach gives

$$f_x^{\mathrm{disl}} \approx 2\mu b\varepsilon_{xy}^{\mathrm{bg}} + M_1\partial_x\varepsilon_{xx}^{\mathrm{bg}} + M_2\partial_x\varepsilon_{yy}^{\mathrm{bg}}. \tag{7.6}$$

This approach predicts that the coefficients appearing in the core force are the moments of $\mathbf{f}^{\mathrm{cf}}(\mathbf{r})$ that appear in the core field. In principle, these moments can be measured by comparing the theoretical dislocation field, which is the sum of the Volterra and core field ones, with the one observed in the crystal, as long as the core field consideration is a good way to correct the Volterra approximation. In the next section, we analyze this through simulation. Unfortunately, we observed that the correct coefficients for the core force measured through simulations, i.e., M_{xx} and M_{yy}, cannot be obtained by the core field analysis.

7.2 FITTING OF VOLTERRA AND CORE FIELD STRAINS

From the core field approach, corrections to the Volterra approximation for the deformations generated by a dislocation can be predicted. We have, for example, that the hydrostatic strain $\varepsilon_{ii} = \varepsilon_{xx} + \varepsilon_{yy}$ generated by a dislocation with $\mathbf{b} = b\,\hat{\mathbf{x}}$ at the origin has the Volterra solution

$$\varepsilon_{ii}^{V}(x,y) = -\frac{(1-\beta)}{\pi}\frac{by}{x^2+y^2} \tag{7.7}$$

and the core field correction (HENAGER JR; HOAGLAND, 2004)

$$\varepsilon_{ii}^{\mathrm{cf}}(x,y) = \frac{M^{\mathrm{dis}}(1-\beta)}{\pi\mu}\frac{(x^2-y^2)}{(x^2+y^2)^2} \tag{7.8}$$

in the dipolar approximation, where $M^{\mathrm{dis}} = (M_2 - M_1)/2$ and M_1 and M_2 are the dipolar moments of $\mathbf{f}^{\mathrm{cf}}(\mathbf{r})$ as defined in the previous section. We can measure the moments of $\mathbf{f}^{\mathrm{cf}}(\mathbf{r})$ by a direct analysis of the strain fields in the real crystal's dislocation compared with the strains given by Volterra and the core field.

In order to analyze the strain fields due to the dislocation alone, we prepared the system of chapter 5 in such a way that:

1. the dipole of dislocations has a separation $d = L_x/2$;
2. a homogeneous strain which cancels the one of equation (3.57) is applied;
3. another horizontal line of particles is included for the system to satisfy the PBC in the $\hat{\mathbf{y}}$-direction.

This results in a simulation cell with $L_x = 192a_0$ and $L_y = 257(\sqrt{3}a_0/2)$ where the dislocations can equilibrate with no need of external sources of strain. We let the system equilibrate without external forces and thereafter translate it in the $\hat{\mathbf{x}}$-direction

until the dislocation with $b = +a_0$ stays at $x = 0$. Only the dislocations themselves and their images are sources of strain.

In the simulation, the strains at each particle position are estimated through the relative positions between it and its neighbors. First, we can compare the real hydrostatic strain field with the Volterra solution which, using equation (7.7) and the results of the end of section 3.2.5, is

$$\begin{aligned}\varepsilon_{ii}^{V}(x,y) &= \sum_{n\in\mathbb{Z},m\in\mathbb{Z}} \left[\varepsilon_{ii}^{\mathrm{V,disl}}(x+nL_x,\ y+mL_y) - \varepsilon_{ii}^{\mathrm{V,disl}}(x+nL_x+L_x/2,\ y+mL_y)\right] \\ &= \frac{2(1-\beta)a_0}{L_x} \sum_{m\in\mathbb{Z}} \mathrm{Im}\left\{\csc\left[2\pi\frac{x+i(y+mL_y)}{L_x}\right]\right\}. \end{aligned} \tag{7.9}$$

As a test, we fit equation (7.9) to the data of the actual strains in the simulation in order to obtain β and compare it with the theoretical value $\beta = 14/19$. Since near the core the Volterra fields are expected to diverge from the real ones, we fitted to the data at positions farther than a cutoff distance r^{c} from the centers of the dislocations. Figure 11 shows how the fitted value for β depends on r^{c}. For $r^{\mathrm{c}} > d/2 \equiv L_x/4$ it fluctuates around a fixed value which is different but near the theoretical one.

Figure 11 – Values for $\beta = B/(B+\mu)$ obtained by fitting equation (7.9) to the hydrostatic strains of the real crystal in the region outside a cutoff distance r^{c} from the centers of the dislocations. As r^{c} increases, it fluctuates around a value near the theoretical prediction $\beta = 14/19 \approx 0.73684$ (green line).

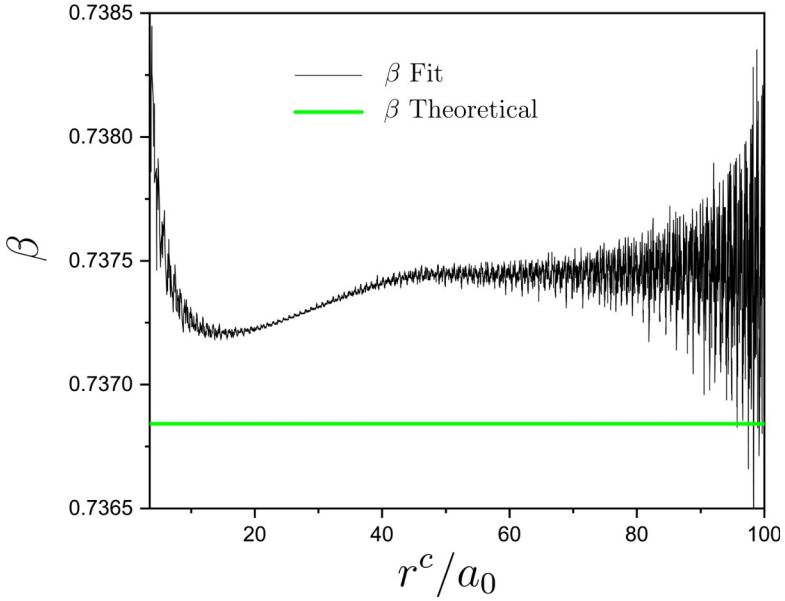

Source: Supplementary Material of (PEREIRA, 2022).

Now we turn to the core field correction which, for a single dislocation, is given by equation (7.8). Then the core field contribution for the total hydrostatic strain is

$$\varepsilon_{ii}^{\mathrm{cf}}(x,y) = \sum_{n\in\mathbb{Z},m\in\mathbb{Z}} \left[\varepsilon_{ii}^{\mathrm{cf,disl}}(x+nL_x,\ y+mL_y) + \varepsilon_{ii}^{\mathrm{cf,disl}}(x+nL_x+L_x/2,\ y+mL_y)\right]$$
$$= \frac{4\pi M^{\mathrm{dis}}(1-\beta)}{\mu L_x^2} \sum_{m\in\mathbb{Z}} \mathrm{Re}\left\{\csc^2\left[2\pi\frac{x+i(y+mL_y)}{L_x}\right]\right\}. \quad (7.10)$$

Moreover, the dislocations can induce a homogeneous ε_{ii}^0 in the system. Figure 12 shows the results for M^{dis} and ε_{ii}^0 from fitting $\varepsilon_{ii}^{\mathrm{cf}} + \varepsilon_{ii}^0$ to the data of the actual strains in the simulation minus the Volterra contribution of equation (7.9). As we can see, far from the core, the fit for M^{dis} converges to a value very different from the one obtained by measuring $(M_{yy} - M_{xx})/2$ in the simulations of core force in chapter 5.

Figure 12 – Values for (a) M^{dis} and (b) ε_{ii}^0 obtained by fitting equation (7.10) plus a constant ε_{ii}^0 to the hydrostatic strains of the real crystal subtracted by equation (7.9). The fit consider points in the region outside a cutoff distance r^{c} from the centers of the dislocations. As r^{c} increases, M^{dis} converges a value different from the one obtained in chapter 5.

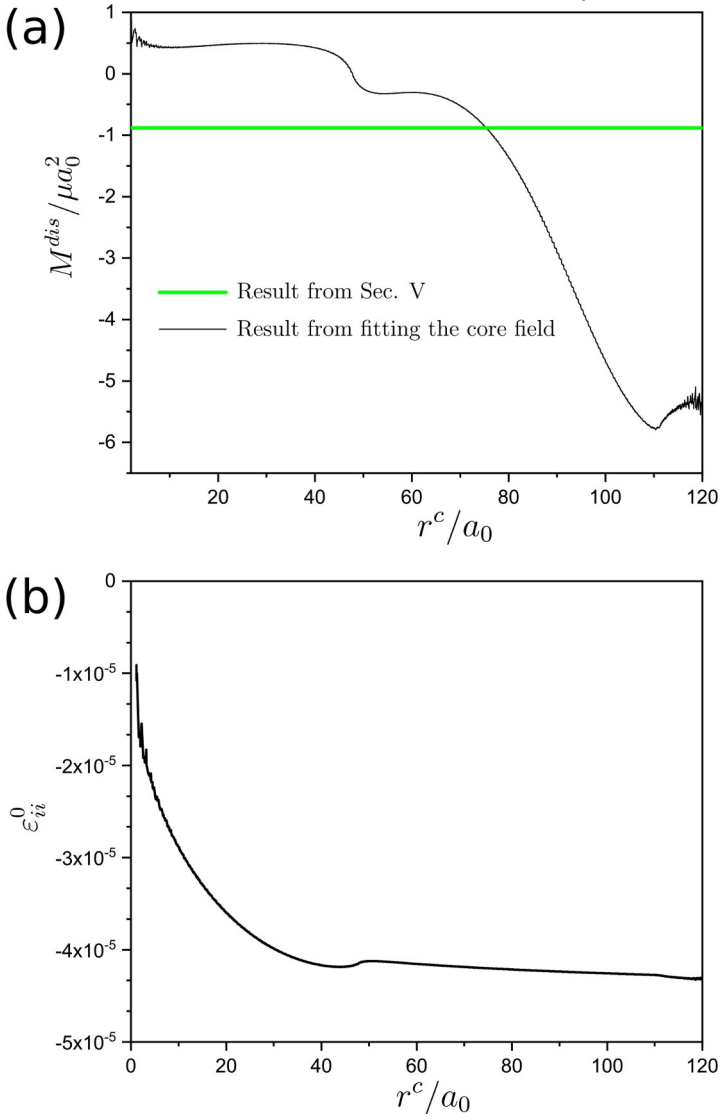

Source: Supplementary Material of (PEREIRA, 2022).

8 FINAL DISCUSSIONS AND CONCLUSIONS

This final chapter reviews and discusses the theoretical and simulational results concerning the core force. Then, it concludes the thesis by overviewing the main novel results and discussing perspectives on possible future works.

8.1 SUMMARY OF COMPARISONS BETWEEN THE THEORIES AND OUR SIMULATIONS

In the previous chapters, we presented some theoretical approaches developed with the aim of providing a correction to the PK force, i.e, the core force. We analyzed if these theories are in agreement with the results of our simulations. Special attention was paid to the physical properties revealed in our simulations, i.e., linearity, locality, symmetry under Burgers vector inversion, uniqueness and effectiveness to drive a dislocation. When possible, quantitative comparisons concerning the core force values were also made.

In this section, we introduce the table 1 in order to present a summary of the comparisons made between the different theories and the results of our simulations. These theories are listed along the first column, the properties are listed from the second to the sixth columns, while the last column refers to the quantitative prediction of the core force (see table 1). For instance, if a given theory obeys a certain property, we signal the table with a “yes”, in the opposite case, we signal it with a “no”.

If a theory does not satisfy a property such as linearity, locality, symmetry or uniqueness, it cannot be the core force observed in our system. Consequently, it does not satisfy the property of effectiveness in our simulations and we cannot make a quantitative investigation about it. The noneffectiveness can be due to several reasons. For instance, Nonlinear Elasticity is expected a priori to be noneffective here since it presumes high deformations for the nonlinear effects to be present, which is not the case in our simulations. In contrast, the assumptions for the SGT that resulted in equation (6.9) expect that it would be present in our simulations, but our results showed no such force since this theory does not satisfy the symmetry that we observed.

Table 1 – Here we list some theoretical approaches that were commented in the previous chapter and predict forces on the dislocations that go beyond the PK force: Nonlinear Elasticity (STEINMANN, 2002), Nonlocal Elasticity (LAZAR, 2005), the Strain Gradient Theory (SGT) of section 6.2 and the core field (CLOUET, 2011) approaches that result in equations (6.9) and (7.6), respectively, and the core energy approach of equation (6.1) that can considerate the standard core energy shown in equation (6.5), as done in (IYER; RADHAKRISHNAN; GAVINI, 2015), or simply a definite ad hoc core energy. In section 5.2, we observe through simulations that a correction to the PK force is needed in order to explain the results. Properties of this correction, such as linearity, locality, symmetry under Burgers vector inversion, uniqueness and driving effectiveness were analyzed and quantitative measures of the force were made. In this table, we compare the theoretical approaches with the results of our simulations, indicating if these theories satisfy the properties and are quantitatively correct.

Theoretical approach	Linear	Local	Symmetric	Unique	Effective	Quantitative
Nonlinear Elasticity	no	yes	no	yes	no	-
Nonlocal Elasticity	yes	no	no	yes	no	-
SGT	yes	yes	no	yes	no	-
Core field	yes	yes	yes	yes	possibly	no
Standard Core Energy	yes	yes	yes	no	no	-
Ad Hoc Core Energy	yes	yes	yes	yes	possibly	no

Source: Adapted from (PEREIRA, 2022).

The Nonlinear Elasticity theory of (STEINMANN, 2002) presumes high deformations in the system. Our simulations used small background strains and, as expected a priori, the linear response of the core force was observed. In addition to nonlinearity, the antisymmetry under $\mathbf{b}$ inversion is also predicted by this theory and was not observed. Thus, such theory is not effective in our case and we could not quantitatively investigate it. But it can be relevant in simulations with high deformations.

The Nonlocal Elasticity theory of (LAZAR, 2005) predicts nonlocal effects in the force when the background strains have high variations within the region around the dislocation. Our simulations have such type of background strain variations, as it can be seen in figure 8, but all the effects observed can be explained locally. In other words, we do not need to know the background strains and their derivatives at other positions but only at the dislocation position. In addition to nonlocality, the antisymmetry under $\mathbf{b}$ inversion is also predicted by the Nonlocal theory and was not observed in our simulations. Thus, such theory is not effective in our case and we

could not quantitatively investigate it. Although unlikely, this theory may be relevant in simulations with other crystal or in 3D.

The results of our simulations are compatible with a force that is linearly proportional to local values of the background strain gradients. This is satisfied by the Strain Gradient Theory (SGT) commented in section 6.2 that results in equation (6.9). But, as we can see directly from the equation, it does not obey the symmetry under Burgers vector inversion that is observed in our simulations. Thus, such theory is not effective in our case and we could not quantitatively investigate it. Although unlikely, this theory may be relevant in simulations with other crystal or in 3D.

It is easy to show that the core field approach, addressed in chapter 7, and used in (CLOUET, 2011), do satisfy some properties (that is, linearity, locality, symmetry and uniqueness) of the core force observed in our simulations. This approach also predicts that the values of the coefficients of the core force (M_{xx}, M_{yy} , ...) are equal to the values of the coefficients of the core field (M_1, M_2, ...). The latter was calculated through fittings of the crystal's deformations with the theoretical ones. We perform such fittings in figure 12 and observe that the fitted value for $(M_2 - M_1)/2$ depends on the fitting region and does not match with $(M_{xx} - M_{yy})/2$ in any meaningful case. Thus, the core field approach prediction is not quantitatively satisfactory. It may possibly have some effectiveness in our system, i.e., either it is wrong or it is true and other type of correction is needed to complement it.

The equation (6.1) gives an approach to obtain the core force through a given core energy, which is taken as a function of the background strains and their derivatives. This approach straightforwardly satisfies the linearity, locality and symmetry properties. If we consider an ad hoc core energy which is unique and gives a core force that quantitatively match the simulational results, then such approach satisfies all the properties of table 1. This is the ultimate theoretical way to describe the core force observed in our simulations. The remaining question is if the ad hoc core energy can be evaluated through other methods. Otherwise we could not predict the core force coefficients without directly measuring them.

The standard way to evaluate the core energy is the one of equation (6.5), but it has ambiguity in the choice of the core radius. Thus, such standard core energy (that was used in (IYER; RADHAKRISHNAN; GAVINI, 2015)) does not satisfies the uniqueness property and then cannot be effective and quantified in our system, which observed a unique core force.

8.2 OVERVIEW OF THE MAIN NOVEL RESULTS AND PERSPECTIVES

In sections 2.1.4 and 2.1.5, as well as during the derivation of equations (3.10) and (3.16), we extensively discussed the necessity of regularization in the continuum approach to elasticity. While we demonstrated a suitable regularization for simple cases, questions persist regarding the limits of its applicability and the optimal choice in the presence of dislocations.

An alternative mathematical formalism for 2D elasticity was proposed in section 2.2.3 and used in sections 2.3, 3.2.3 and 3.2.4. This formalism yielded simpler equations and provided physical insights in specific cases. In principle, its utility may extend to other scenarios and could potentially be generalized to 3D.

In section 4.1.5, when examining the core force, we noted its nonreciprocal property in the interaction between identical dislocations. Witnessing this phenomenon in action would be intriguing. For instance, configurations might exist where two dislocations perpetually drive each other in a specific direction.

The challenges faced in observing and precisely measuring the effects of the core force in simulations were outlined section 4.2.1. We proposed a simulation model, which was implemented in chapter 5. While additional difficulties may arise in experiments and 3D simulations, it is likely feasible to overcome them to some extent of precision.

In section 3.2.3, through the analysis of energy and Peach-Koehler force expressions, we deduced the existence and structure of conformal crystals. Considering the effective influence of core forces, it might be possible to detect their signatures in the final configuration of the few remaining dislocations in the conformal crystal, given the presence of relevant strain gradients in such crystals.

Our simulation results proved to be at odds with predictions from established theoretical approaches, as extensively discussed in the last two chapters and summarized in the previous section. In an attempt to reconcile discrepancies, we conducted an additional simulation for one of these approaches—the core field method—in section 7.2. However, it was not able to predict the correct core force coefficients.

In principle, three potential avenues of research may hold promise in providing good predictions, although these endeavors have faced challenges thus far. To achieve analytical predictions, researchers can explore modifications to the energy

functional or to the description of dislocations within continuum theory. Alternatively, efforts could be directed towards developing an appropriate method for measuring the core energy, enabling a semi-analytical approach to predict the core force. Notably, in section 6.1.3, we took a reverse approach, obtaining the core energy in our system from the results of the core force. Comparing this energy with other measurement methods may yield valuable physical insights.

REFERENCES

AIFANTIS, Elias C. On the role of gradients in the localization of deformation and fracture. **International Journal of Engineering Science**, v. 30, n. 10, p. 1279-1299, 1992.

BRAGG, W. L.; NYE, J. F. A dynamical model of a crystal structure. **Proceedings of the Royal Society of London. Series A. Mathematical and Physical Sciences**, v. 190, n. 1023, p. 474-481, 1947.

BULATOV, V.; CAI, W. **Computer Simulations of Dislocations**. Oxford: OUP, 2006.

BRAVERMAN, Lara et al. Topological defects in solids with odd elasticity. **Physical Review Letters**, v. 127, n. 26, p. 268001, 2021.

CLOUET, Emmanuel. Dislocation core field. I. Modeling in anisotropic linear elasticity theory. **Physical Review B**, v. 84, n. 22, p. 224111, 2011.

DAS, Sambit; GAVINI, Vikram. Electronic structure study of screw dislocation core energetics in Aluminum and core energetics informed forces in a dislocation aggregate. **Journal of the Mechanics and Physics of Solids**, v. 104, p. 115-143, 2017.

ERINGEN, A. Cemal. **Nonlocal Continuum Field Theories**. New York: Springer-Verlag, 2002.

FLECK, N. A.; HUTCHINSON, J. W.; WILLIS, J. R. Guidelines for constructing strain gradient plasticity theories. **Journal of Applied Mechanics**, v. 82, n. 7, p. 071002, 2015.

FRANK, F. Crystal growth and dislocations. **Advances in Physics**, v. 1, n. 1, p. 91-109, 1952.

GAO, Yanfei; BEI, Hongbin. Strength statistics of single crystals and metallic glasses under small stressed volumes. **Progress in Materials Science**, v. 82, p. 118-150, 2016.

GREER, Julia R.; DE HOSSON, J. T. M. Plasticity in small-sized metallic systems: Intrinsic versus extrinsic size effect. **Progress in Materials Science**, v. 56, n. 6, p. 654-724, 2011.

GURRUTXAGA-LERMA, Beñat. The role of the mobility law of dislocations in the plastic response of shock loaded pure metals. **Modelling and Simulation in Materials Science and Engineering**, v. 24, n. 6, p. 065006, 2016.

GURRUTXAGA-LERMA, Benat; VERSCHUEREN, Jonas. Generalized Kanzaki force field of extended defects in crystals with applications to the modeling of edge dislocations. **Physical Review Materials**, v. 3, n. 11, p. 113801, 2019.

HENAGER JR, Charles H.; HOAGLAND, Richard G. Dislocation core fields and forces in FCC metals. **Scripta Materialia**, v. 50, n. 7, p. 1091-1095, 2004.

HIRTH, J. P.; LOTHE, J. **Theory of Dislocations**. New York: Wiley, 1982.

HU, Yi et al. Atomistic dislocation core energies and calibration of non-singular discrete dislocation dynamics. **Modelling and Simulation in Materials Science and Engineering**, v. 28, n. 1, p. 015005, 2019.

HUANG, Y. et al. A conventional theory of mechanism-based strain gradient plasticity. **International Journal of Plasticity**, v. 20, n. 4-5, p. 753-782, 2004.

HUTCHINSON, John; FLECK, Norman. Strain gradient plasticity. **Advances in Applied Mechanics**, v. 33, p. 295-361, 1997.

IRANI, Nilgoon et al. Effect of dislocation core fields on discrete dislocation plasticity. **Mechanics of Materials**, v. 165, p. 104137, 2022.

IYER, Mrinal; RADHAKRISHNAN, Balachandran; GAVINI, Vikram. Electronic-structure study of an edge dislocation in aluminum and the role of macroscopic deformations on its energetics. **Journal of the Mechanics and Physics of Solids**, v. 76, p. 260-275, 2015.

KAPFER, Sebastian C.; KRAUTH, Werner. Two-dimensional melting: From liquid-hexatic coexistence to continuous transitions. **Physical Review Letters**, v. 114, n. 3, p. 035702, 2015.

KRAFT, Oliver et al. Plasticity in confined dimensions. **Annual Review of Materials Research**, v. 40, p. 293-317, 2010.

KUBIN, L. **Dislocations, Mesoscale Simulations and Plastic Flow**. Oxford: Oxford University Press, 2013.

LAZAR, Markus. Peach-Koehler forces within the theory of nonlocal elasticity. In: **Mechanics of Material Forces**. Boston: Springer US, 2005. p. 149-158.

LAZAR, Markus; KIRCHNER, Helmut O. K. The Eshelby stress tensor, angular momentum tensor and dilatation flux in gradient elasticity. **International Journal of Solids and Structures**, v. 44, n. 7-8, p. 2477-2486, 2007.

LOOS, Sarah AM; KLAPP, Sabine HL. Irreversibility, heat and information flows induced by non-reciprocal interactions. **New Journal of Physics**, v. 22, n. 12, p. 123051, 2020.

MENEZES, Raí M.; SILVA, Clécio C. de Souza. Conformal vortex crystals. **Scientific Reports**, v. 7, n. 1, p. 12766, 2017.

MENG, Qingyou; GRASON, Gregory M. Defects in conformal crystals: Discrete versus continuous disclination models. **Physical Review E**, v. 104, n. 3, p. 034614, 2021.

MEYERS, M. A. et al. Dislocations in shock compression and release. **Dislocations in Solids**, v. 15, p. 91-197, 2009.

MIGUEL, M. C.; ZAPPERI, S. Tearing transition and plastic flow in superconducting thin films. **Nature Materials**, v. 2, n. 7, p. 477-481, 2003.

MISHRA, Avanish et al. Fingerprinting shock-induced deformations via diffraction. **Scientific Reports**, v. 11, n. 1, p. 9872, 2021.

NABARRO, F. R. N. Dislocations in a simple cubic lattice. **Proceedings of the Physical Society**, v. 59, n. 2, p. 256, 1947.

NOSENKO, V.; MORFILL, G. E.; ROSAKIS, P. Direct experimental measurement of the speed-stress relation for dislocations in a plasma crystal. **Physical Review Letters**, v. 106, n. 15, p. 155002, 2011.

PEACH, M.; KOEHLER, J. S. The forces exerted on dislocations and the stress fields produced by them. **Physical Review**, v. 80, n. 3, p. 436, 1950.

PEIERLS, R. The size of a dislocation. **Proceedings of the Physical Society**, v. 52, n. 1, p. 34, 1940.

PEREIRA, P. C. N.; APOLINÁRIO, S. W. S. Forces on dislocations due to strain gradients: Theories and two-dimensional simulations. **Physical Review B**, v. 106, n. 22, p. 224105, 2022.

PHILLIPS, R. **Crystals, Defects And Microstructures: Modeling Across Scales**. Cambridge: Cambridge University Press, 2001.

PIERAŃSKI, P. Gravity's rainbow-structure of a 2d crystal grown in a strong gravitational field. In: **Phase Transitions In Soft Condensed Matter**. Boston: Springer US, 1989. p. 45-48.

PIZZAGALLI, L.; DEMENET, J.-L.; RABIER, J. Theoretical study of pressure effect on the dislocation core properties in semiconductors. **Physical Review B**, v. 79, n. 4, p. 045203, 2009.

PO, Giacomo et al. A non-singular theory of dislocations in anisotropic crystals. **International Journal of Plasticity**, v. 103, p. 1-22, 2018.

PONCET, Alexis; BARTOLO, Denis. When soft crystals defy newton's third law: Nonreciprocal mechanics and dislocation motility. **Physical Review Letters**, v. 128, n. 4, p. 048002, 2022.

REMINGTON, Bruce A.; RUDD, Robert E.; WARK, Justin S. From microjoules to megajoules and kilobars to gigabars: Probing matter at extreme states of deformation. **Physics of Plasmas**, v. 22, n. 9, 2015.

SATOH, A. **Introduction to practice of molecular simulation: Molecular Dynamics, Monte Carlo, Brownian Dynamics, Lattice Boltzmann and Dissipative Particle Dynamics**. Amsterdam: Elsevier, 2011.

SILVA, Fillipe C. O. et al. Formation and stability of conformal spirals in confined 2D crystals. **Journal of Physics: Condensed Matter**, v. 32, n. 50, p. 505401, 2020.

SLIWA, M. et al. Femtosecond X-ray diffraction studies of the reversal of the microstructural effects of plastic deformation during shock release of tantalum. **Physical Review Letters**, v. 120, n. 26, p. 265502, 2018.

STEINMANN, Paul. On spatial and material settings of hyperelastostatic crystal defects. **Journal of the Mechanics and Physics of Solids**, v. 50, n. 8, p. 1743-1766, 2002.

STRANDBURG, Katherine J. Two-dimensional melting. **Reviews of Modern Physics**, v. 60, n. 1, p. 161, 1988.

TAYLOR, G. I. The mechanism of plastic deformation of crystals. Part I.—Theoretical. **Proceedings of the Royal Society of London. Series A, Containing Papers of a Mathematical and Physical Character**, v. 145, n. 855, p. 362-387, 1934.

VAN DER MEER, B. et al. Highly cooperative stress relaxation in two-dimensional soft colloidal crystals. **Proceedings of the National Academy of Sciences**, v. 111, n. 43, p. 15356-15361, 2014.

VANSADERS, Bryan; DSHEMUCHADSE, Julia; GLOTZER, Sharon C. Strain fields in repulsive colloidal crystals. **Physical Review Materials**, v. 2, n. 6, p. 063604, 2018.

VAULINA, O. S.; LISINA, I. I.; LISIN, E. A. Energy exchange in systems of particles with nonreciprocal interaction. **Journal of Experimental and Theoretical Physics**, v. 121, p. 717-726, 2015.

VOLTERRA, V. Sur l'équilibre des corps élastiques multiplement connexes. In: **Annales Scientifiques De L'école Normale Supérieure**. 1907. p. 401-517.

VOYIADJIS, George Z.; SONG, Yooseob. Strain gradient continuum plasticity theories: theoretical, numerical and experimental investigations. **International Journal of Plasticity**, v. 121, p. 21-75, 2019.

VOYIADJIS, George Z.; YAGHOOBI, Mohammadreza. Review of nanoindentation size effect: Experiments and atomistic simulation. **Crystals**, v. 7, n. 10, p. 321, 2017.

VOYIADJIS, George Z; YAGHOOBI, Mohammadreza. **Size Effects in Plasticity: from Macro to Nano**. [S.l.]: Academic Press, 2019.

WEHRENBERG, Christopher E. et al. In situ X-ray diffraction measurement of shock-wave-driven twinning and lattice dynamics. **Nature**, v. 550, n. 7677, p. 496-499, 2017.

ZAISER, Michael; SANDFELD, Stefan. Scaling properties of dislocation simulations in the similitude regime. **Modelling and Simulation in Materials Science and Engineering**, v. 22, n. 6, p. 065012, 2014.

ZEPEDA-RUIZ, Luis A. et al. Probing the limits of metal plasticity with molecular dynamics simulations. **Nature**, v. 550, n. 7677, p. 492-495, 2017.